Astronomy & Astrophysics manuscript no. astroph
February 5, 2008
© ESO 2008

arXiv:astro-ph/0607264v1 12 Jul 2006

Abundance analysis of prime B-type targets for asteroseismology

I. Nitrogen excess in slowly-rotating β Cephei stars ⋆

T. Morel[1,⋆⋆], K. Butler[2], C. Aerts[1,3], C. Neiner[1,4], and M. Briquet[1]

[1] Katholieke Universiteit Leuven, Departement Natuurkunde en Sterrenkunde, Instituut voor Sterrenkunde, Celestijnenlaan 200B, B-3001 Leuven, Belgium
[2] Universitäts-Sternwarte München, Scheinerstrasse 1, D-81679 München, Germany
[3] Department of Astrophysics, University of Nijmegen, PO Box 9010, 6500 GL Nijmegen, The Netherlands
[4] GEPI, UMR 8111 du CNRS, Observatoire de Paris-Meudon, 5 place Jules Janssen, 92195 Meudon Cedex, France

Received 9 March 2006 / Accepted 8 July 2006

ABSTRACT

Context. Seismic modelling of the β Cephei stars promises major advances in our understanding of the physics of early B-type stars on (or close to) the main sequence. However, a precise knowledge of their physical parameters and metallicity is a prerequisite for correct mode identification and inferences regarding their internal structure.

Aims. Here we present the results of a detailed NLTE abundance study of nine prime targets for theoretical modelling: γ Peg, δ Cet, ν Eri, β CMa, ξ^1 CMa, V836 Cen, V2052 Oph, β Cep and DD (12) Lac (hereafter 12 Lac). The following chemical elements are considered: He, C, N, O, Mg, Al, Si, S and Fe.

Methods. Our curve-of-growth abundance analysis is based on a large number of time-resolved, high-resolution optical spectra covering in most cases the entire oscillation cycle of the stars.

Results. Nitrogen is found to be enhanced by up to 0.6 dex in four stars, three of which have severe constraints on their equatorial rotational velocity, ΩR, from seismic or line-profile variation studies: β Cep (ΩR~26 km s^{-1}), V2052 Oph (ΩR~56 km s^{-1}), δ Cet ($\Omega R < 28$ km s^{-1}) and ξ^1 CMa ($\Omega R \sin i \lesssim 10$ km s^{-1}). The existence of core-processed material at the surface of such largely unevolved, slowly-rotating objects is not predicted by current evolutionary models including rotation. We draw attention to the fact that three stars in this subsample have a detected magnetic field and briefly discuss recent theoretical work pointing to the occurrence of diffusion effects in β Cephei stars possibly capable of altering the nitrogen surface abundance. On the other hand, the abundances of all the other chemical elements considered are, within the errors, indistinguishable from the values found for OB dwarfs in the solar neighbourhood. Despite the mild nitrogen excess observed in some objects, we thus find no evidence for a significantly higher photospheric metal content in the studied β Cephei stars compared to non-pulsating B-type stars of similar characteristics.

Key words. stars: early-type – stars: fundamental parameters – stars: abundances – stars: atmospheres – stars: oscillations

1. Introduction

The class of the β Cephei pulsating variables is defined as B0–B3 V–III stars excited by both (low-order) pressure and gravity modes. The concommitant existence of these two types of modes, along with their relatively simple internal structure, offers the prospect of probing their deep interiors via detailed seismic modelling. This will allow stringent constraints on some fundamental parameters of early B-type dwarfs and subgiants, such as the extent of convective core overshooting or the rotation law in the radiative envelope, to be set in the near future. Although forthcoming or space missions already in operation (e.g. *MOST*, *COROT*) are expected to lead to dramatic advances in this field, very intensive ground-based observations have already demonstrated the potential of such techniques (Dupret et al. 2004).

The unstable modes in β Cephei stars are driven by the κ-mechanism and arise from an opacity bump at $T \sim 2 \times 10^5$ K in their interior. It immediately follows that the incidence of pulsations is predicted to be largely controlled by the metal content, with the instability domains in the Hertzprung-Russell (HR) diagram shrinking or even completely vanishing in the low metallicity regimes (Pamyatnykh 1999; Deng & Xiong

Send offprint requests to: T. Morel, e-mail: thierry@ster.kuleuven.be.

⋆ Table A.1 is only available in electronic form at the CDS via anonymous ftp to cdsarc.u-strasbg.fr (130.79.128.5) or via http://cdsweb.u-strasbg.fr/cgi-bin/qcat?J/A+A/???/???

⋆⋆ European Space Agency (ESA) postdoctoral external fellow.

2001). However, recent pieces of evidence suggest that our understanding of the excitation mechanisms in these stars is likely to be still incomplete. First, the number of β Cephei candidates in the LMC is much higher than theoretically predicted (Kołaczkowski et al. 2004). Second, current pulsation models have increasing difficulties in accounting for all the frequencies detected in some key objects as more and more intensive observational campaigns are undertaken (e.g. 12 Lac: Handler et al. 2006; ν Eri: Pamyatnykh et al. 2004; Ausseloos et al. 2004). Non-standard stellar models including gravitational settling and radiative levitation might need to be invoked in such cases, as first suggested by Pamyatnykh et al. (2004).

These inconsistencies between theory and observations will be better appraised when the physical parameters (especially $T_{\rm eff}$) and chemical composition (i.e. stellar opacities) of these objects are precisely known. Noteworthy attempts to determine the effective temperature and global metallicity of several β Cephei stars from *International Ultraviolet Explorer (IUE)* data have recently been presented (Niemczura & Daszyńska-Daszkiewicz 2005), but more robust estimates are likely to be obtained from a detailed analysis of high-quality optical data. Furthermore, a knowledge of the abundances of the individual chemical species is preferable in the context of theoretical modelling, as early-type stars may present significant departures from a scaled solar mixture. In particular, rotationally-induced mixing can lead to the dredge up of some core-processed CNO material in fast-rotating, main-sequence OB stars (e.g. Meynet & Maeder 2000; Proffitt & Quigley 2001). Such deviations from the standard solar abundance pattern might be routinely incorporated in the near future in any evolution and pulsation codes, and their impact on the pulsational properties explored (see Ausseloos 2005).

Notwithstanding the ease with which high-quality spectroscopic data can be gathered for such bright objects, surprisingly little attention has been paid in recent years to derive the stellar parameters and abundances of β Cephei stars from high-resolution optical spectra, with the only dedicated studies going back to the early 70s (Watson 1971, 1972; Peters 1973). It is the goal of this project to remedy this situation by taking advantage of the dramatic improvement in data quality, atmospheric models and non-LTE (NLTE) modelling techniques. Here we present a pilot study of nine archetypical β Cephei stars, describing in detail the methodology used to derive the atmospheric parameters and elemental abundances in a self-consistent way. The next papers in this series will be devoted to a sample of Slowly Pulsating B stars (SPBs) and to the OB-type stars within reach of the asteroseismology programme of the *COROT* mission (Baglin 2003).

2. Observational material

Most of the selected stars have been the subject of very intensive (multisite) campaigns over the last few years, both in photometric and spectroscopic modes. As such, they are amongst the β Cephei stars (and indeed early-type stars) with the highest number of pulsation modes identified and are thus ideally suited for further theoretical modelling (e.g. ν Eri: Ausseloos et al. 2004; V836 Cen: Aerts et al. 2003). Table 1 summarizes the basic pulsation properties of our targets. Most of the stars with a dominant radial mode do not possess large-amplitude non-radial modes, except ν Eri. On the other hand, the radial mode is excited in the three stars with a dominant non-radial mode, but with a lower amplitude.

Table 1. Basic pulsation properties of our targets. $N(\nu)$: number of independent pulsation frequencies detected. Data from stated papers and references therein.

Star	Dominant pulsation mode	$N(\nu)$	Most recent reference
γ Peg	Radial	4	Chapellier et al. (2006)
δ Cet	Radial	4	Aerts et al. (2006)
ν Eri	Radial	14	Jerzykiewicz et al. (2005)
β CMa	Non-radial	3	Desmet et al. (2006)
ξ^1 CMa	Radial	1	Saesen et al. (2006)
V836 Cen	Non-radial	6	Aerts et al. (2004b)
V2052 Oph	Radial	2	Neiner et al. (2003)
β Cep	Radial	5	Telting et al. (1997)
12 Lac	Non-radial	11	Handler et al. (2006)

A description of the spectroscopic data used is given in Table 2. Further details on the data acquisition and reduction procedures can be found in Aerts et al. (2004a; ν Eri), Mazumdar et al. (2006; β CMa), Saesen et al. (2006; ξ^1 CMa), Aerts et al. (2004b; V836 Cen), Neiner et al., in prep. (V2052 Oph) and Desmet et al., in prep. (12 Lac). The data for δ Cet were obtained at ESO during the 2002 July 17–25 period and were reduced with a dedicated reduction software for the CORALIE spectrograph (see Baranne et al. 1996). The spectra of γ Peg and β Cep have been retrieved from the ELODIE archives (see Moultaka et al. 2004). Aerts et al. (2004b) presented a preliminary spectral synthesis analysis of V836 Cen based on a spectrum reduced with the FEROS reduction pipeline. The raw data have been completely re-reduced here with standard `IRAF`[1] tasks, resulting in a much higher data quality.

Our analysis for each star is based on a mean spectrum generally created by co-adding a large number of individual exposures (up to 579; Table 2). These spectra were put in the laboratory rest frame prior to forming the weighted (by the S/N ratio) average of the whole time series, as large radial velocity variations are often observed. The orders of the mean spectrum were then merged using `IRAF` tasks. Sections of the merged spectrum were subsequently continuum normalized by fitting the line-free regions with low-order cubic spline polynomials. Each individual echelle order was separately normalized for the data acquired with the CS2 spectrograph at McDonald observatory, as the merging procedure proved unsatisfactory in that case.

The very high signal-to-noise ratio often attained for the combined spectrum enables us to confidently measure weak diagnostic lines. Figure 1 illustrates this point for some Fe III features and allows one to get a sense of the overall data qual-

[1] `IRAF` is distributed by the National Optical Astronomy Observatories, operated by the Association of Universities for Research in Astronomy, Inc., under cooperative agreement with the National Science Foundation.

Table 2. Basic description of the spectroscopic data. Spectral types from the SIMBAD database (revised values are given in Table 7). $\Delta\lambda$: spectral range covered in Å, R: mean resolving power of the spectrograph, N: number of exposures combined, S/N: typical signal-to-noise ratio at about 4500 Å in the *individual* exposures (estimated from photon statistics).

	γ Peg	δ Cet	ν Eri	β CMa	ξ^1 CMa[a]		V836 Cen	V2052 Oph	β Cep	12 Lac
					Max EWs	Min EWs				
HD number	HD 886	HD 16582	HD 29248	HD 44743	HD 46328		HD 129 929	HD 163 472	HD 205 021	HD 214 993
Spectral type	B2 IV	B2 IV	B2 III	B1 II/III	B1 III		B3 V	B2 IV–V	B2 IIIevar	B2 III
Telescope	1.9-m OHP	1.2-m Euler	1.2-m Euler	1.2-m Euler	1.2-m Euler		2.2-m Euler	2.7-m McDonald	1.9-m OHP	2.7-m McDonald
Instrument	ELODIE	CORALIE	CORALIE	CORALIE	CORALIE		FEROS	CS2	ELODIE	CS2
$\Delta\lambda$	3895–6820	3875–6820	3875–6820	3875–6820	3875–6820		3555–9215	3630–10 275	3895–6820	3630–10 275
R	50 000	50 000	50 000	50 000	50 000		48 000	60 000	50 000	60 000
N	47	4	579	449	38	41	1	105	28	31
S/N	215	150	250	250	180	200	150	230	215	285

[a] Min and Max EWs correspond to minimum and maximum EWs of the Si III lines, respectively.

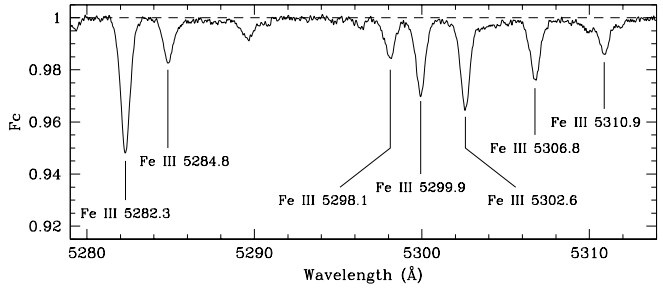

Fig. 1. Mean, normalized spectrum of β CMa in the spectral range 5279–5314 Å. Some weak Fe III lines are indicated.

ity. More importantly, combining such a large number of time-resolved spectra also allows us to minimize the impact of the strong line-profile variations arising from pulsations (see Aerts et al. 1994 for some examples) and the related changes in the equivalent widths (EWs), which are, for instance, typically of the order of 3–4% for the Si III lines in β Cephei stars (De Ridder et al. 2002). All the fundamental quantities we derive (e.g. $T_{\rm eff}$) can thus be regarded in most cases as representative of the mean values averaged over the pulsation cycles. This is one of the most important aspects of the present work with respect to previous studies based on snapshot spectra (e.g. Gies & Lambert 1992; hereafter GL). In the case of ξ^1 CMa, the excellent time sampling and relatively simple nature of the pulsations (only a large-amplitude radial mode is excited) prompted us to examine the phase-related changes in the atmospheric parameters. To this end, we separately analyzed two mean spectra created for two phase intervals of width $\Delta\phi$=0.1 corresponding to minimum and maximum EWs of the Si III lines (see Saesen et al. 2006).

3. Method of analysis

3.1. Model atmosphere calculations and spectral synthesis

We made use of the latest versions of the NLTE line formation codes DETAIL and SURFACE originally developed by Butler (1984) and Giddings (1981), along with plane-parallel, fully line-blanketed LTE Kurucz atmospheric models (Kurucz 1993). Grids with solar metallicity were used. Slight deviations from the solar mixture for some metals (e.g. N; see below) do not have an appreciable effect on the atmospheric structure. We adopted models with He/H=0.089 by number in all cases, in accordance with the derived helium abundances. The only exception was V2052 Oph, as it displays some evidence for a helium enrichment (see Sect. 4 and Neiner et al. 2003).

We used Kurucz Opacity Distribution Functions (ODFs) with a fine frequency mesh (1212 points). To limit computational time, we adopted a constant microturbulent velocity, $\xi_{\rm mod}$=8 km s^{-1}, in the statistical equilibrium calculations with DETAIL. This value is in most cases consistent with the microturbulence derived from the line analysis. Test calculations for β CMa show that the exact choice of this parameter has little impact on the final results, with the mean abundance differences being less than 0.05 dex for all elements when adopting $\xi_{\rm mod}$=2 or 8 km s^{-1}.

The following chemical elements are considered: He, C, N, O, Mg, Al, Si, S and Fe. The number of levels for the various ionic species is provided in Table 3, along with the original literature sources where basic information on the model atoms can be found. Note that the atomic data used (e.g. photoionization cross sections) have been regularly updated following advances in theoretical calculations. The Fe III model atom will be described in detail in a forthcoming paper (Butler et al., in prep.). Here we note that the bulk of the atomic data, energy levels, oscillator strengths and damping parameters are taken from Kurucz (1993). While the Fe II and Fe IV atoms are rudimentary, the Fe III model includes all terms calculated to lie below the ionization threshold.

The line atomic data (e.g. oscillator strengths, radiative damping constants) are taken from the NIST[2] or VALD (Kupka et al. 1999) databases. The NLTE populations are computed assuming LS coupling. Our line list includes most of the diagnostic lines generally used in abundance analyses of early B-type stars, but great care has been taken to only retain unblended features for the relevant temperature ranges.[3] Our final line list is made up of about 180 spectral lines.

[2] Available online at: `http://physlab2.nist.gov/PhysRefData/ASD/index.html`.

[3] We made extensive use of the spectral atlases for main-sequence B stars available at: `http://www.lsw.uni-heidelberg.de/cgi-bin/websynspec.cgi` (see Gummersbach et al. 1998).

Table 3. Number of levels for the various ions having their populations explicitely treated in NLTE with DETAIL. The ground states of C IV, N IV, O IV, Mg III, Al IV, Si V, S IV and Fe V are also considered.

Ion	Number of levels	Reference
H I	10	Husfeld et al. (1989)
He I	27	Husfeld et al. (1989)
He II	14	
C II	54	Eber & Butler (1988)
C III	3	
N I	3	Becker & Butler (1989)
N II	50	
N III	5	
O I	3	Becker & Butler (1988)
O II	52	
O III	3	
Mg I	88	Przybilla et al. (2001)
Mg II	37	
Al III	12	Dufton et al. (1986)
Si II	34	Trundle et al. (2004), see also text
Si II	28	
Si IV	18	
S II	78	Vrancken et al. (1996)
S III	21	
Fe II	8	Butler et al., in prep.
Fe III	264	
Fe IV	16	

As will be shown in Sect. 4, the programme stars span a restricted range in $T_{\rm eff}$ and $\log g$. This implies that the departures from LTE should be roughly uniform among our sample and the relative abundances fairly insensitive to the treatment of NLTE line formation. Extremely few NLTE iron abundance studies of early B-type stars have been presented in the literature (to our knowledge, the only one being the analysis of the B1.5 dwarf HD 35299 by Vrancken 1997). The magnitude of the NLTE corrections affecting the Fe III lines, $\Delta\epsilon=(\log\epsilon)_{\rm NLTE}-(\log\epsilon)_{\rm LTE}$, hence deserves further discussion. The departures from LTE are found to negligible for the coolest objects in our sample ($\Delta\epsilon \lesssim +0.05$ dex), but to significantly increase with $T_{\rm eff}$ (e.g. $\Delta\epsilon$=+0.21 dex for β Cep and +0.33 dex for ξ^1 CMa, respectively). Previous LTE values in the literature derived from Fe III lines for B1 dwarfs or earlier subtypes can thus be regarded as strict lower limits. For the other elements, an illustrative LTE abundance analysis carried out on β CMa suggests systematically negative mean NLTE corrections never exceeding 0.17 dex (see Table 4). Such modest departures from LTE for early B-type dwarfs or subgiants explains the reasonable agreement with past LTE abundance determinations in the literature (e.g. Martin 2004 and Rolleston et al. 2003 in the case of γ Peg and ξ^1 CMa, respectively); large discrepancies can generally be ascribed to other factors, such as differences in the adopted atmospheric parameters or atomic data.

Table 4. NLTE corrections in the case of β CMa. The number of lines considered is given in brackets. Note that the listed corrections for some ions are based on very few lines and may not be representative.

Element	Ion	$\Delta\epsilon=(\log\epsilon)_{\rm NLTE}-(\log\epsilon)_{\rm LTE}$
C	C II (8)	–0.07
	C III (1)	0.00
	C II+C III (9)	–0.06
N	N II (25)	–0.11
	N III (1)	0.00
	N II+N III (26)	–0.11
O	O II (30)	–0.14
Mg	Mg II (2)	–0.10
Al	Al III (4)	0.00
Si	Si II (2)	+0.03
	Si III (6)	–0.26
	Si IV (1)	–0.06
	Si II+Si III+Si IV (9)	–0.17
S	S II (1)	+0.10
	S III (1)	–0.12
	S II+S III (2)	–0.01
Fe	Fe III (25)	+0.09

3.2. Estimate of atmospheric parameters

The stellar physical parameters were derived in a standard way, whereby $T_{\rm eff}$ and $\log g$ are self-consistently determined using an iterative scheme. Few iterations are needed before convergence is attained when sensible starting values can easily be estimated a priori, as is the case here. The effective temperature was estimated from the Si II/III/IV ionization equilibrium. Unfortunately, the spectral lines of these three ions are only measurable in β CMa and β Cep. For the other stars, we had to solely rely on the Si II/III or Si III/IV lines. This has motivated us to replace the 12-level Si II model ion initially implemented in DETAIL (Becker & Butler 1990) by a more complete atomic model with 34 levels developed by D. J. Lennon. This is expected to allow for a more realistic treatment of the ionization balance and leads to a slightly cooler temperature scale (see Trundle & Lennon 2005). Figure 2 provides various examples of calibrations between the Si line ratios and $T_{\rm eff}$. We used solar Si abundances (as appropriate for our stars; see below) and atmospheric models with a $\xi_{\rm mod}$ value matching as closely as possible the microturbulence estimated from the line analysis. Several line ratios (up to 12 in total) were used for the temperature determination. Not all of them are completely independent (only seven transitions are involved), but consistent results were obtained in all cases. The dispersion between the obtained values was taken as representative of the temperature uncertainty. This proved to be comparable from star to star and of the order of 1000 K. In cases where the abundances of C, N and S are based on lines of two adjacent ionization stages, no convincing evidence for systematic discrepancies was found. As a result, all abundances yielded by the individual lines were averaged irrespective of their ionization stage. This gives credence to the reliability of our temperature scale, although the scope of such a comparison is limited by the coarse treatment of the minor ionic species C III and N III in our model atoms

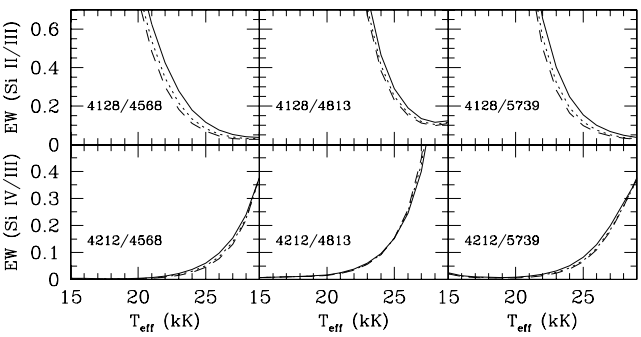

Fig. 2. Examples of calibrations between various Si line ratios and the effective temperature, as a function of ξ. The dependence on the microturbulence must in certain cases be taken into account, as the lines used may be of very different strength. Solid line: ξ=5 km s^{-1}; dotted line: ξ=10 km s^{-1}; dashed line: ξ=15 km s^{-1}. In this case we adopted $\log g$=3.5 [cgs], $\log \epsilon$(Si)=7.20 dex and $\xi_{\rm mod}$=8 km s^{-1}.

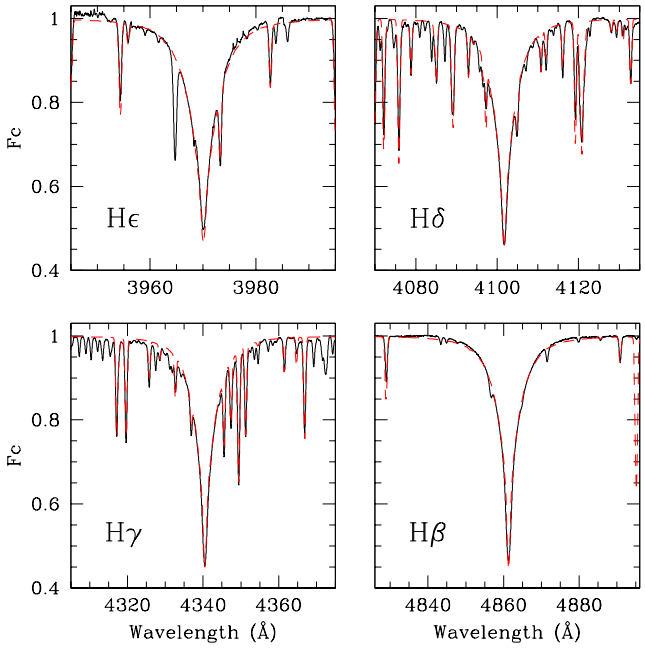

Fig. 3. Synthetic (*dotted line*; $T_{\rm eff}$=24 000 K and $\log g$=3.5 [cgs]) and observed (*solid line*) spectra of β CMa for the regions encompassing the Balmer lines.

(Table 3). We will comment further on this point in Sect. 4.1 by comparing our $T_{\rm eff}$ values with literature data.

The surface gravity was derived by fitting the collisionally-broadened wings of the Balmer lines. Line broadening mechanisms such as rotation or microturbulence only affect the line cores and hence no prior knowledge of these quantities is needed. The Hβ line was not used in β Cep, as the Hα profile is clearly filled-in by a variable emission component. Hβ may thus slightly be affected by emission as well. All of Hϵ, Hδ, Hγ and Hβ were used for the other stars, as the lower series members are unlikely to be substantially affected by circumstellar/wind emission. Indeed, they systematically yielded consistent results, as can be seen in Fig. 3 in the case of β CMa. Typical uncertainties are of the order of 0.15–0.20 dex and reflect both the dispersion of the values obtained using the various lines, errors arising from the uncertainty on the $T_{\rm eff}$ calibration and imperfections in the merging of the echelle orders. As mentioned in Sect. 2, this step in the reduction procedure was not possible for the McDonald data. Therefore, the profile fitting of the Balmer lines in V2052 Oph was performed using spectra obtained with the Coudé Echelle spectrograph mounted on the 2-m telescope of the Tautenburg observatory, Germany (see Neiner et al., in prep.). For 12 Lac, we made use of a snapshot spectrum extracted from the ELODIE archives.

The microturbulence, ξ, was estimated by requiring the abundances yielded by the individual O II lines to be independent of the line strength. To estimate the uncertainties, we varied this parameter until the slope of the $\log \epsilon$(O)-$\log(EW/\lambda)$ relation differs from zero at the 3σ level. The oxygen features are the strongest metal lines in our spectra and are thus best suited for this purpose. However, the microturbulent velocities obtained from the N II lines are much lower than those obtained from the O II features for the most massive objects (β CMa, ξ^1 CMa, β Cep and 12 Lac) and are in better agreement with the values inferred for B-type stars in general using other methods (e.g. Fitzpatrick & Massa 2005). Although extensively discussed in the literature, the possible causes of these inconsistencies remain unclear (e.g. Trundle et al. 2004; see also Sect. 5.1). We provide in Table 5 some illustrative examples of the abundance differences resulting from the exact choice of the species used to determine the microturbulence. Although we note that adopting the low values suggested by the N II lines would lead to unreasonably high abundances for several strong lines of other elements, we cannot rule out a systematic, albeit slight ($\Delta \log \epsilon \lesssim 0.2$ dex), underestimate of the stellar abundances in some objects.

Table 5. Abundance differences when adopting the microturbulent velocities yielded by the N II lines (ξ=2 and 3 km s^{-1} for ξ^1 CMa and β Cep, respectively) instead of the default values derived from the O II features (ξ=6 km s^{-1} in both cases).

	ξ^1 CMa	β Cep
$\Delta\xi$	from 6 to 2 km s^{-1}	from 6 to 3 km s^{-1}
ΔHe/H	+0.014	+0.005
$\Delta \log \epsilon$(C)	+0.02	+0.01
$\Delta \log \epsilon$(N)	+0.08	+0.05
$\Delta \log \epsilon$(O)	+0.20	+0.13
$\Delta \log \epsilon$(Mg)	+0.18	+0.14
$\Delta \log \epsilon$(Al)	+0.10	+0.06
$\Delta \log \epsilon$(Si)	+0.09	+0.17
$\Delta \log \epsilon$(S)	+0.04	+0.02
$\Delta \log \epsilon$(Fe)	+0.06	+0.04

3.3. Estimate of chemical abundances

The abundances are derived once the atmospheric parameters mentioned above are known by matching the measured EWs of the selected lines (tabulated in Table A.1) and the values measured in the synthetic spectra. Such an EW-based abundance analysis is made possible by the fact that all our stars are rel-

Table 6. Calculation of the error budget in the case of β CMa. $\sigma_{\rm int}$: line-to-line scatter; $\sigma_{T_{\rm eff}}$: variation of the abundances for $\Delta T_{\rm eff}$=+1000 K; $\sigma_{\log g}$: as before, but for $\Delta \log g$=+0.15 dex; σ_{ξ}: as before, but for $\Delta\xi$=+3 km s^{-1}; $\sigma_{T_{\rm eff}/\log g}$: as before, but for $\Delta T_{\rm eff}$=+1000 K and $\Delta \log g$=+0.15 dex; σ_T: total uncertainty.

	$\sigma_{\rm int}$	$\sigma_{T_{\rm eff}}$	$\sigma_{\log g}$	σ_{ξ}	$\sigma_{T_{\rm eff}/\log g}$	σ_T
ΔHe/H	0.014	0.010	0.007	0.020	0.003	0.028
$\Delta \log \epsilon$(C)	0.037	0.074	0.001	0.019	0.059	0.103
$\Delta \log \epsilon$(N)	0.121	0.046	0.008	0.026	0.042	0.139
$\Delta \log \epsilon$(O)	0.088	0.078	0.040	0.109	0.053	0.174
$\Delta \log \epsilon$(Mg)	0.156	0.060	0.015	0.050	0.050	0.182
$\Delta \log \epsilon$(Al)	0.096	0.093	0.022	0.032	0.060	0.152
$\Delta \log \epsilon$(Si)	0.206	0.036	0.009	0.086	0.028	0.228
$\Delta \log \epsilon$(S)	0.212	0.100	0.035	0.015	0.060	0.245
$\Delta \log \epsilon$(Fe)	0.178	0.033	0.031	0.015	0.046	0.190

atively slow rotators, as will be shown below. For consistency, direct integration was used in both cases. In a few instances, multicomponent fitting using a Voigt profile was performed with IRAF tasks in the case of well-separated blends.

Five sources of error on the final abundances were considered. Apart from the line-to-line scatter[4] ($\sigma_{\rm int}$), we first calculated the errors arising from the uncertainties on the atmospheric parameters ($\sigma_{T_{\rm eff}}$, $\sigma_{\log g}$ and σ_{ξ}). They were derived by computing the abundances using models with atmospheric parameters deviating from the final values by the relevant uncertainties. We also took into account the fact that the determinations of $T_{\rm eff}$ and $\log g$ are strongly coupled ($\sigma_{T_{\rm eff}/\log g}$). The other covariance terms do not significantly contribute to the total error budget and can be neglected. Finally, we quadratically add these errors to obtain the total uncertainty, σ_T. Table 6 illustrates these calculations in the case of β CMa. It can be seen that the accuracy of the abundance determination varies significantly depending upon the element considered, being typically of the order of 0.1 dex for C, but much larger for S and Si, for instance (~0.2–0.3 dex). This primarily reflects the sensitivity to changes in the physical parameters, limitations in the model atoms, as well as inaccuracies in the atomic data.

A comment is necessary regarding the helium abundance determination in V2052 Oph. This star has been classified as He-strong by Neiner et al. (2003) who obtained He/H=0.21 by number based on a detailed NLTE analysis of a number of optical He I lines. Although our curve-of-growth analysis does not support such a high helium content (see below), contrary to the other stars in our sample we were unable to obtain consistent fits for all the He I lines considered. In particular, it was impossible to fit the wings of the diffuse lines using a single helium abundance, some lines being well fit with He/H=0.09, others with twice the solar value (particularly the singlets). Interestingly, a similar phenomenon is observed in β Cep. A detailed investigation is beyond the scope of this paper, but this phenomenon may be related to the existence of surface inhomogeneities/vertical stratification of helium in these two magnetic stars. As mentioned in Sect. 3.1, Kurucz models with He/H=0.178 have been used for V2052 Oph. This choice has a negligible impact on the atmospheric parameters and abundances (ΔHe/H=0.003; $\Delta \log \epsilon \lesssim 0.05$ dex).

[4] The Mg abundance was often derived from a single line. In this case, we fixed $\sigma_{\rm int}$ to 0.15 dex.

3.4. Estimate of the amount of line broadening

We provide in Table 7 a total line broadening parameter, v_T, defined as:

$$v_T^2 = (\Omega R \sin i)^2 + v_{\rm macro}^2 + v_{\rm puls}^2, \quad (1)$$

with Ω the equatorial angular rotational frequency, R the stellar radius, i the inclination angle, $v_{\rm macro}$ the macroturbulent velocity and $v_{\rm puls}$ the amount of pulsational line broadening averaged over the oscillation cycle. The latter is expected to be significant for non-radial modes, but to be small for radial pulsators (cf. comparison between Tables 1 and 7). The amount of macroturbulent broadening is unknown for our objects which are on, or close to, the main sequence. The v_T values were estimated as a final step of the abundance analysis by fitting the profiles of some isolated O II lines with a grid of synthetic spectra with the appropriate microturbulent velocity and convolved with a rotational broadening profile (Gray 1976), assuming a limb-darkening coefficient, ϵ=0.4 (Claret 2000). The instrumental profile was estimated from calibration lamps.

To disentangle the effect of rotational and macroturbulent broadening on the one hand, and of the averaged pulsational line broadening on the other hand, we have selected the spectrum least affected by pulsations in the time series, i.e. with the narrowest and most symmetric line profiles (this is not possible for V836 Cen, as we only have one observation). These were used to derive the quantity: $(\Omega R \sin i)^2 + v_{\rm macro}^2$. The amount of averaged pulsational line broadening immediately follows from Eq. 1. The true stellar rotation rates, ΩR, are known for most targets (Sect. 5.3) and indicate that some macroturbulence does seem to occur in some stars (see Table 7).

4. Results and comparison with previous studies

4.1. Physical parameters

The atmospheric parameters of the programme stars are presented in Table 7. We also provide the revised MK spectral types based on our $T_{\rm eff}$ estimates and the spectral type-$T_{\rm eff}$ calibration for Galactic OB dwarfs of Crowther (1998). It is necessary to assess the reliability of our derived $T_{\rm eff}$ and $\log g$ estimates before discussing the chemical properties of our targets. An exhaustive literature search was not attempted. Instead, a comparison was made with atmospheric parameters obtained using three independent methods: (i) $T_{\rm eff}$ primarily derived from Strömgren photometry and $\log g$ from profile fitting of Hγ (GL); (2) both parameters estimated from Walraven colour indices, or from Geneva and Strömgren photometry when these data were not available (Heynderickx et al. 1994); (iii) temperatures based on the continuum fitting of low-resolution *IUE* data (Niemczura & Daszyńska-Daszkiewicz 2005). As can be seen in Fig. 4, our temperatures (and consequently surface gravities) are systematically lower than the values quoted by GL, but

Table 7. Physical parameters of the programme stars. The revised MK spectral types are based on our $T_{\rm eff}$ estimates and the calibration of Crowther (1998). The 1-σ uncertainty on $T_{\rm eff}$ and $\log g$ are 1000 K and 0.15 dex, respectively (except for V836 Cen and V2052 Oph: $\Delta \log g$=0.20 dex).

	γ Peg	δ Cet	ν Eri	β CMa	ξ^1 CMa		V836 Cen	V2052 Oph	β Cep	12 Lac
					Max EWs	Min EWs				
Revised spectral type	B1.5–B2 V	B1.5–B2 V	B1.5–B2 V	B1.5 V–IV	B0.5–B1 V–IV		B1.5 V	B1.5–B2 V	B1 Vevar	B1.5 V
$T_{\rm eff}$ (K)	22 500	23 000	23 500	24 000	27 000	28 000	24 500	23 000	26 000	24 500
$\log T_{\rm eff}$ (K)	4.352±0.019	4.362±0.019	4.371±0.019	4.380±0.018	4.431±0.016	4.447±0.016	4.389±0.018	4.362±0.019	4.415±0.017	4.389±0.018
$\log g$ (cm s^{-2})	3.75	3.80	3.75	3.50	3.70	3.80	3.95	4.00	3.70	3.65
ξ (km s^{-1})	1^{+2}_{-1}	1^{+3}_{-1}	10±4	14±3	6±2		6±3	1^{+4}_{-1}	6±3	10±4
v_T (km s^{-1})	10	14	36	23	10		15	62	29	42
$\left[(\Omega R \sin i)^2 + v^2_{\rm macro}\right]^{1/2}$ (km s^{-1})	~10	~13	~16	~20	~10			~61	~29	~37
$v_{\rm puls}$ (km s^{-1})	negligible	negligible	~32	~11	negligible			negligible	negligible	~20
ΩR (km s^{-1})		14 or 28[a]	6[a]	32[b]			2[a]	56[c]	26[c]	45[b]
$v_{\rm macro}$ (km s^{-1})		?	$\gtrsim$ 15	?				$\gtrsim$ 20	$\gtrsim$ 10	?

[a] From seismic studies (Dupret et al. 2004; Pamyatnykh et al. 2004; Aerts et al. 2006).
[b] From modelling of the line-profile variations (the so-called "moment method"; Aerts 1996, Desmet et al. 2006).
[c] Calculated from the stellar radius derived from evolutionary tracks (Fig. 5) and assuming that the rotational period can be identified with the recurrence timescale of the changes affecting the UV lines: $\mathcal{P}_{\rm rot}$=12.001 06 d in β Cep (Henrichs et al. 2000) and 3.638 833 d in V2052 Oph (Neiner et al. 2003).

there are reasons to believe that their temperature scale is too hot. In particular, they applied a systematic upward correction to their temperatures in order to match the empirical calibration derived by Code et al. (1976) from angular diameter and absolute flux measurements. However, more recent and accurate observations (Smalley & Dworetsky 1995) lead to systematically lower values by about 1000 K in this temperature range (see discussion in Lyubimkov et al. 2002). The star β CMa was incidentally included in this sample of standard stars and is ideally suited for a direct comparison: $T_{\rm eff}$ was decreased from 25 180±1130 (Code et al. 1976) to 24 020±1150 K (Smalley & Dworetsky 1995), which is now in better agreement with our results. Additionally, we note that Aufdenberg et al. (1999) obtained absolutely identical values to ours for $T_{\rm eff}$ and $\log g$ from the fitting of the spectral energy distribution from the near-UV to the infrared using a fully line-blanketed, spherical and NLTE atmospheric model. On the other hand, our $T_{\rm eff}$ values tend to be slightly higher than those obtained from colour indices. The photometric calibrations in the Walraven photometric system are based on the grids of lightly line-blanketed model atmospheres of Kurucz (1979). Unfortunately, the lack of further details (e.g. zero points) does not allow us to identify the cause of these discrepancies. Better agreement is found with the temperatures derived from UV data, but large differences are found for our two hottest objects: ξ^1 CMa and β Cep. As regards the surface gravities, our values are identical, within the errors, to those presented by Heynderickx et al. (1994).

A variation $\Delta T_{\rm eff}$~1000 K and $\Delta \log g$~0.1 dex is inferred during the radial pulsation cycle of ξ^1 CMa. This is comparable to the uncertainties, but the changes in the EWs of temperature-sensitive lines (Table A.1) are such that the temperature variations are clearly real. Furthermore, Beeckmans & Burger (1977) obtained very similar results from UV colour indices: $\Delta T_{\rm eff}$=1400±430 K. This can be compared to values obtained by various means for other β Cephei stars dominated by a large-amplitude radial mode: e.g., $\Delta T_{\rm eff}$=4000±2000 K and $\Delta \log g$=0.7±0.4 dex for σ Sco (van der Linden & Butler 1988), $\Delta T_{\rm eff}$=900±120 K for V2052 Oph (Morton & Hansen 1974) or $\Delta T_{\rm eff}$~1200 K for δ Cet (De Ridder et al. 2002).

4.2. Stellar abundances

The mean NLTE abundances are given in Table 8, along with the resulting metallicity, Z. As a consistency check, we have repeated the abundance analysis of ξ^1 CMa for the two phase ranges considered, finding nearly identical results in both cases. A detailed abundance analysis has been performed for seven stars in our sample by GL. However, a detailed comparison is probably not warranted for the following reasons: (a) the two sets of atmospheric parameters adopted are systematically different, with their temperature scale being likely too hot (see discussion above); (b) the NLTE corrections applied are based on atmospheric models with an inadequate treatment of metal line blanketing (Gold 1984). Nitrogen being of particular relevance (see below), we simply note the perhaps fortuitous close agreement between the NLTE abundances, with differences never exceeding 0.2 dex. Ignoring previous LTE studies (e.g. Watson 1971; Peters 1973), the same quantitative agreement is found for γ Peg, δ Cet and V2052 Oph with other NLTE CNO abundance determinations in the literature (Andrievsky et al. 1999; Korotin et al. 1999a,b,c; Neiner et al. 2003).

5. Discussion

5.1. Neglect of stellar winds

It is natural to ask to what extent the results presented in this paper are robust against the neglect of the stellar wind, particularly in view of the fact that the inferred microturbulent velocities are in some cases comparable to the sound velocity in the O II line-forming regions (recall that an overestimate of this parameter would lead to spuriously low abundances). As expected, relaxing the assumption of LTE leads to a decrease of this quantity, but relatively large values are still obtained with a full NLTE treatment. In the case of β CMa, for instance, ξ decreases from 18 to only 14 km s^{-1} when NLTE is enforced. Furthermore, although our sample is admittedly small and the range in surface gravity limited, there is an indication for higher microturbulent velocities in the more evolved objects (see also Kilian 1992 and Daflon et al. 2004). It is tempting to interpret

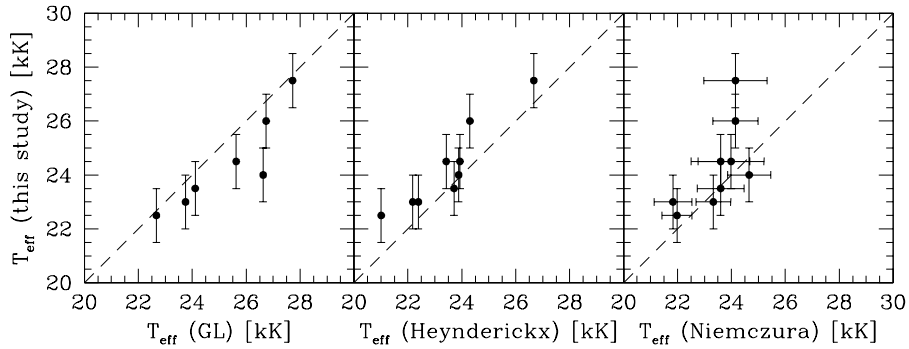

Fig. 4. Comparison between our $T_{\rm eff}$ values and literature data.

Table 8. Mean NLTE abundances, along with the total 1-σ uncertainties, σ_T (by convention, $\log\epsilon$[H]=12). The number of used lines is given in brackets. For comparison purposes, the last four columns give: the unweighted mean values for our sample (Mean), typical values found for OB dwarfs in the solar neighbourhood (Daflon & Cunha 2004; OB stars), the standard solar composition of Grevesse & Sauval (1998; Sun 1-D), and finally solar abundances recently derived from 3-D hydrodynamical models (Asplund et al. 2005; Sun 3-D). The metallicity, Z, is calculated assuming that the abundances of the elements not under study is solar (Grevesse & Sauval 1998). We define [N/C] and [N/O] as $\log[\epsilon({\rm N})/\epsilon({\rm C})]$ and $\log[\epsilon({\rm N})/\epsilon({\rm O})]$, respectively.

	γ Peg	δ Cet	ν Eri	β CMa	ξ^1 CMa		V836 Cen	V2052 Oph
					Max EWs	Min EWs		
He/H	0.079±0.025 (9)	0.096±0.024 (10)	0.076±0.024 (8)	0.070±0.028 (9)	0.098±0.017 (10)	0.099±0.016 (10)	0.078±0.024 (10)	0.118±0.032 (9)
$\log\epsilon$(C)	8.20±0.05 (8)	8.09±0.08 (6)	8.24±0.12 (10)	8.16±0.11 (9)	8.19±0.11 (9)	8.17±0.12 (9)	8.34±0.13 (8)	8.21±0.07 (4)
$\log\epsilon$(N)	7.58±0.11 (23)	8.05±0.11 (26)	7.87±0.09 (18)	7.59±0.14 (26)	8.00±0.16 (34)	7.99±0.18 (34)	7.73±0.10 (21)	7.99±0.17 (10)
$\log\epsilon$(O)	8.43±0.28 (21)	8.45±0.26 (19)	8.51±0.24 (19)	8.62±0.18 (30)	8.59±0.16 (34)	8.59±0.17 (34)	8.49±0.24 (25)	8.39±0.30 (14)
$\log\epsilon$(Mg)	7.44±0.25 (1)	7.52±0.29 (1)	7.38±0.24 (1)	7.30±0.18 (2)	7.37±0.20 (1)	7.38±0.20 (1)	7.41±0.19 (3)	7.35±0.32 (1)
$\log\epsilon$(Al)	6.12±0.16 (4)	6.13±0.21 (4)	6.08±0.16 (4)	6.00±0.15 (4)	6.16±0.21 (4)	6.16±0.23 (4)	6.13±0.11 (4)	6.09±0.24 (2)
$\log\epsilon$(Si)	7.19±0.29 (6)	7.28±0.29 (6)	7.21±0.26 (9)	7.17±0.23 (9)	7.14±0.23 (4)	7.12±0.19 (4)	7.14±0.19 (9)	7.16±0.37 (6)
$\log\epsilon$(S)	7.22±0.20 (14)	7.26±0.24 (4)	7.32±0.22 (5)	7.14±0.25 (2)	6.98±0.11 (2)	7.00±0.21 (2)	7.39±0.26 (2)	7.32±0.21 (5)
$\log\epsilon$(Fe)	7.25±0.16 (28)	7.32±0.18 (21)	7.36±0.19 (17)	7.17±0.19 (25)	7.31±0.19 (32)	7.28±0.25 (32)	7.30±0.09 (16)	7.37±0.21 (9)
Z	0.0091±0.0021	0.0100±0.0021	0.0105±0.0022	0.0104±0.0021	0.0110±0.0018	0.0108±0.0020	0.0105±0.0022	0.0097±0.0022
[N/C]	–0.62±0.12	–0.04±0.14	–0.37±0.15	–0.57±0.18	–0.19±0.20	–0.18±0.22	–0.61±0.17	–0.22±0.19
[N/O]	–0.85±0.30	–0.40±0.29	–0.64±0.26	–1.03±0.23	–0.59±0.23	–0.60±0.25	–0.76±0.26	–0.40±0.35

	β Cep	12 Lac	Mean	OB stars	Sun 1-D	Sun 3-D
He/H	0.078±0.028 (8)	0.075±0.031 (8)	0.085±0.015	0.10[a]	0.085	0.085
$\log\epsilon$(C)	8.02±0.10 (11)	8.22±0.12 (6)	8.18±0.09	~8.2	8.52	8.39
$\log\epsilon$(N)	7.91±0.13 (19)	7.64±0.18 (17)	7.82±0.19	~7.6	7.92	7.78
$\log\epsilon$(O)	8.47±0.14 (30)	8.42±0.23 (22)	8.49±0.08	~8.5	8.83	8.66
$\log\epsilon$(Mg)	7.31±0.21 (1)	7.29±0.23 (1)	7.37±0.07	~7.4	7.58	7.53
$\log\epsilon$(Al)	6.02±0.16 (4)	6.11±0.17 (3)	6.09±0.05	~6.1	6.47	6.37
$\log\epsilon$(Si)	7.11±0.23 (8)	7.11±0.27 (6)	7.17±0.05	~7.2	7.55	7.51
$\log\epsilon$(S)	7.14±0.37 (2)	7.10±0.31 (2)	7.21±0.13	~7.2	7.33	7.14
$\log\epsilon$(Fe)	7.24±0.23 (23)	7.30±0.20 (22)	7.29±0.06	~7.4[b]	7.50	7.45
Z	0.0091±0.0013	0.0089±0.0018	0.0099±0.0007	~0.0099	0.0172	0.0124
[N/C]	–0.11±0.17	–0.58±0.22	–0.36±0.21	~–0.6	–0.60	–0.61
[N/O]	–0.56±0.19	–0.78±0.29	–0.67±0.21	~–0.9	–0.91	–0.88

[a] From Lyubimkov et al. (2004). The primordial helium abundance is He/H~0.08 (e.g. Olive & Skillman 2004).
[b] Mean NLTE abundance of four BA supergiants in the solar vicinity (Przybilla et al. 2006).

these high microturbulences as an artefact of our assumption of a hydrostatic photosphere (e.g. Lamers & Achmad 1994). However, there is ample evidence in the literature indicating that high microturbulent velocities are needed, even when state-of-the-art, "unified" codes accounting for mass loss and spherical extension are used (e.g. Mokiem et al. 2005).

A number of studies have investigated in recent years the differences between the atmospheric parameters and/or abundances of early-type stars obtained using the plane-parallel code TLUSTY (Hubeny & Lanz 1995) and the unified codes CMFGEN/FASTWIND (Hillier & Miller 1998; Puls et al. 2005). This comparison was performed for a small sample of Galactic/SMC B-type supergiants (Urbaneja et al. 2003; Trundle et al. 2004; Dufton et al. 2005) and Galactic O-type dwarfs (Bouret et al. 2005; Martins et al. 2005). The differences were claimed to be of the order of the uncertainties and hence of no significance. These consistency checks support the validity of our analysis, especially considering that weaker winds by at least two orders of magnitude are expected in our sample. Perhaps of more relevance is the fact that the same conclusion was reached for some late O-type dwarfs in the SMC having mass-loss rates comparable to what is anticipated for β Cephei stars ($\dot{M}$ down to 10^{-9}–10^{-10} $M_\odot$ yr^{-1}; Bouret et al. 2003). A very weak wind was derived for the most evolved star in our sample, β CMa, from soft X-ray observations: $\dot{M}$=6 $\times$ 10^{-9} $M_\odot$ yr^{-1} (Drew et al. 1994).

In summary, although forthcoming analyses of our programme stars using unified models would obviously be desirable, the choice of the line formation code used is very unlikely to affect our conclusions about the abundance patterns and does not alleviate our concerns regarding the high microturbulent velocities.

5.2. Abundance patterns

As can be seen in Table 8, the abundances of He, C, O, Mg, Al, Si and Fe span a limited range in the studied stars (less than 0.3 dex). This is comparable to the total uncertainties and indicates that the abundances of these species are remarkably uniform among our sample. The homogeneous nature of our sample in terms of spectral type implies that our results should be fairly insensitive to several sources of systematic errors. Nevertheless, we verified that no significant trends exist between the abundances and $T_{\rm eff}$. This important check supports the reliability of our NLTE corrections and temperature scale and in turn partly explains the small scatter within our sample. Nitrogen and sulphur exhibit a significantly larger spread of the order of 0.4–0.5 dex. The S abundances are derived from very few lines (sometimes of different ionization stages), which suggests that this scatter may not have a physical basis. On the contrary, we will argue below that the star-to-star N variations are real and may be interpreted in terms of mixing processes (Sect. 5.3).

One issue we wish to address with the present study is the possible existence of a dichotomy between the chemical properties of the β Cephei stars and those of non-pulsating early B-type stars. In the following we shall use the mean abundance of OB stars in the solar neighbourhood as a baseline for comparison purposes. The final results of a comprehensive, homogeneous abundance study of about 90 late O- to early B-type Galactic stars on (or close to) the main sequence have recently been presented by Daflon & Cunha (2004). The analysis is similar in several aspects to our study (use of DETAIL/SURFACE and Kurucz models), a fact which reduces the systematic errors. The typical abundances at the solar galactocentric distance (all our stars lie within 1 kpc) are quoted for all the elements in Table 8, along with the mean values for our sample.[5] A direct comparison shows a near-perfect agreement for He, C, O, Mg, Al, Si and S. Our mean LTE iron abundance (~7.18 dex) is in reasonable agreement with the value of ~7.3 dex estimated by Daflon et al. (1999, 2001a) for early B-type dwarfs. However, we prefer to compare our results to the NLTE Fe abundances of four relatively nearby ($d \lesssim 3$ kpc) late-B to early-A supergiants obtained by Przybilla et al. (2006) using a set of optical Fe II lines and the model atom developed by Becker (1998). The Fe abundance is not altered during the evolution of massive stars, allowing for a meaningful comparison. Our mean NLTE abundance is slightly lower than the value quoted by Przybilla et al. (2006), but is still compatible when taking the errors into account (Table 8).

[5] It is customary in seismic studies to use the standard solar mixtures of Grevesse & Sauval (1998) or more recent values based on 3-D hydrodynamical models, as summarized by Asplund et al. (2005). These values are also quoted for convenience in Table 8.

5.3. Evidence for deep mixing

As stated above, nitrogen is the chemical species exhibiting the largest star-to-star spread. This may indicate the existence in some stars of the products of (incomplete) CNO-cycle burning brought to the surface by deep internal mixing. Evolutionary effects are known to greatly enhance the photospheric N abundance in BA supergiants, but fast rotation leading to meridional currents and shear instabilities in the interior is widely believed to be responsible for mixing prior to the first dredge-up in single early-type stars. The positions of the programme stars in the HR diagram are displayed in Fig. 5. This shows that our targets are largely unevolved and have masses ranging from about 9 to 20 $M_{\odot}$. The most recent evolutionary models including rotation suggest that fast-rotating B stars in this mass range could display a measurable N excess of the order of a few tenths of a dex at the end of the main sequence. This should be accompanied by a slight C depletion at the 0.1 dex level, which is comparable to our uncertainties and therefore barely detectable. On the other hand, He and O should remain virtually unaffected (Heger & Langer 2000; Meynet & Maeder 2003). The signature of deep mixing in the stellar interior can be best revealed by examining the abundance ratios between N, C and O ([N/C] and [N/O]; see Table 8). This shows that γ Peg, β CMa, V836 Cen and 12 Lac have ratios typical of both nearby OB stars and the Sun, whereas δ Cet, ξ^1 CMa, V2052 Oph, β Cep and to a much lesser extent ν Eri display higher values by up to 0.6 dex (a factor 4). The two subsamples of N-normal and N-rich stars are separated by about 0.5 dex in terms of the [N/C] ratio (which is the most robust diagnostic for an N enrichment), i.e. about three times the typical uncertainty in the determination of this quantity (Table 8). The exact choice of the chemical species used to derive the microturbulence (oxygen or nitrogen) has little impact on these conclusions, as the [N/C] and [N/O] ratios are affected by at most 0.12 dex in the case of ξ^1 CMa and β Cep (see Table 5).

Such abundance patterns are in line with the predictions of the theoretical models cited above and support the idea that some objects are indeed experiencing substantial rotationally-induced mixing. Boron abundances are available for seven stars in our sample and can be used to further examine the relevance of this interpretation (Proffitt & Quigley 2001; Venn et al. 2002; Mendel et al. 2006). This fragile element is destroyed by proton capture at relatively low temperatures ($T \sim 4 \times 10^6$ K) and is already completely depleted throughout most of the stellar envelope during the very early phases of evolution off the zero-age main sequence (ZAMS). The boron surviving in the outer stellar layers will quickly be transported downwards and be destroyed at the onset of rotational mixing. This will be followed by an increase of the nitrogen content as core-processed gas is being gradually mixed to the surface. As a result, one expects the N-rich stars to be most severely B depleted and, conversely, the stars with little B depletion to have near-solar N

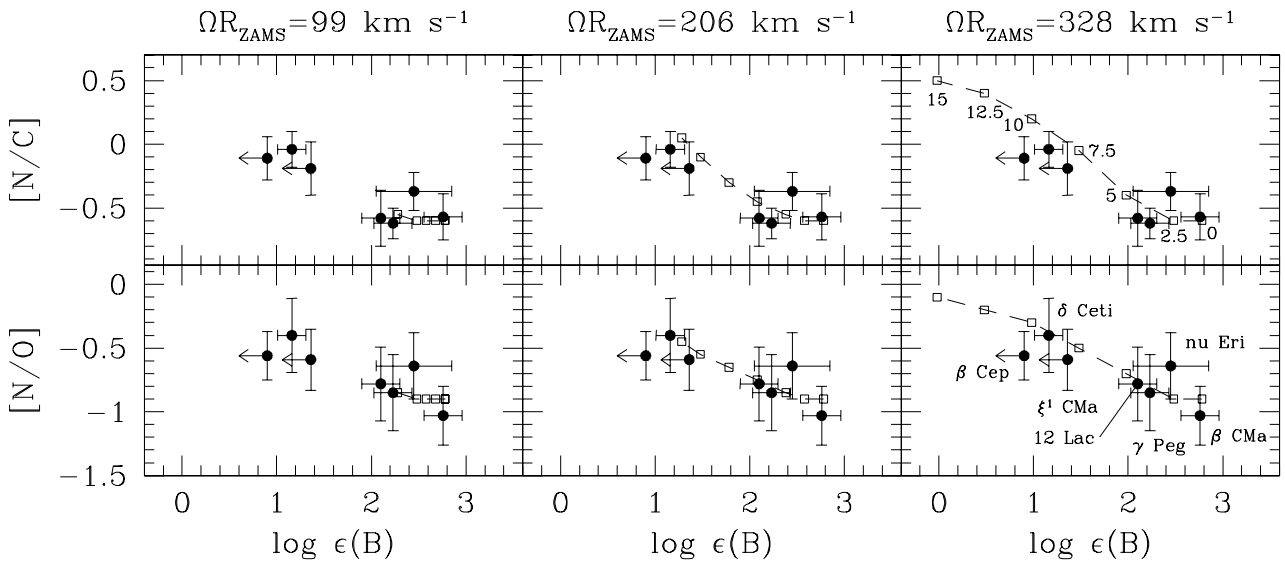

Fig. 6. [N/C] and [N/O] ratios as a function of the NLTE B abundances. The boron data are primarily taken from Proffitt & Quigley (2001), but have been complemented in the case of δ Cet, β Cep and 12 Lac by more stringent estimates from the literature (Venn et al. 2002; Mendel et al. 2006). The arrows denote upper limits. The abundance data are compared to the theoretical predictions of Heger & Langer (2000) for a 12 $M_{\odot}$ star and three different values of the equatorial rotational velocity on the ZAMS: $\Omega R_{\rm ZAMS}$=99 (*left-hand panels*), 206 (*middle panels*) and 328 km s^{-1} (*right-hand panels*). The locus in each panel (*dashed line and open squares*) defines an age sequence with the time elapsed from the ZAMS increasing leftwards: from t=0 to 15 Myrs (0 to 12.5 Myrs for $\Omega R_{\rm ZAMS}$=99 km s^{-1}) by steps of 2.5 Myrs (see upper-right panel). The initial [N/C], [N/O], and boron abundances at t=0 have been taken as: –0.6, –0.9 (Table 8) and log ϵ(B)=2.78±0.04 (meteoritic value; Zhai & Shaw 1994), respectively.

abundances. This is consistent with the situation depicted in Fig. 6.

However, high initial rotational velocities are required to reproduce the observed abundance patterns. For instance, an initial rotational velocity on the ZAMS, $\Omega R_{\rm ZAMS}$, of about 200 km s^{-1} is necessary to account for the N excess in δ Cet (with an age of about 14 Myrs according to evolutionary tracks; Fig. 5). The loss of angular momentum along the main sequence leads to a decrease of the rotation rate, but ΩR is still expected to be in this case of the order of 150 km s^{-1} at the end of core H burning (Heger & Langer 2000; Meynet & Maeder 2003). This is in excellent agreement with the observations of early-B dwarfs in young open clusters, which reveal only a slow decline of the rotation rate from ~170 km s^{-1} on the ZAMS to ~130 km s^{-1} at the end of core-hydrogen burning (Huang & Gies 2006). Most stars enriched in nitrogen have just evolved off the main sequence (Fig. 5), such that reproducing the observed abundance ratios requires high rotational velocities. This is in stark contrast with the fact that none of our targets is apparently rapidly rotating ($\Omega R \sin i$ < 65 km s^{-1}; Table 7).

Comparisons between the surface abundances of the products of nucleosynthesis and the predictions of models accounting for mass loss and rotation are usually performed in a statistical sense (e.g. Herrero & Lennon 2004) and rely on the determination of CNO abundances for a large sample of stars only having an estimate of their *projected* rotational velocity. One of the key features of this study is that the *true* rotation rates, ΩR, have been estimated for several of our targets by a detailed modelling of either the line-profile variations or the pulsation spectrum (see Table 7), offering an opportunity to constrain the models in a more quantitative way. First, seismic modelling of ν Eri and V836 Cen has revealed a non-rigid rotation profile with very low equatorial velocities of about 6 and 2 km s^{-1}, respectively (Dupret et al. 2004; Pamyatnykh et al. 2004). *MOST* observations of δ Cet also lead to a likely rotational velocity of about 28 km s^{-1}, or half this value depending on the exact mode identification (Aerts et al. 2006). Second, modelling of the line-profile variations yields ΩR=32 and 45 km s^{-1} in β CMa and 12 Lac, respectively (Desmet et al. 2006; Aerts 1996). In addition, assuming that the periodicity of the changes affecting the UV lines can be identified with the rotational period (Neiner et al. 2003; Henrichs et al. 2000), leads to ΩR~56 and 26 km s^{-1} in V2052 Oph and β Cep, respectively. Although this quantity is unfortunately unknown for ξ^1 CMa, this shows that at least three N-rich stars (δ Cet, V2052 Oph and β Cep) are intrinsically slow rotators and should not exhibit any abundance peculiarities according to evolutionary models.

Meridional currents are believed to be the most important mechanism governing the loss of angular momentum in (non-magnetic) B stars experiencing little mass loss, while shear mixing arising from differential rotation largely controls the transport of the chemical elements (Meynet & Maeder 2000). The observed discrepancy between the observations and the theoretical predictions could imply that the treatment of these two physical processes is still approximate in evolutionary models including rotation. It is also conceivable, for instance,

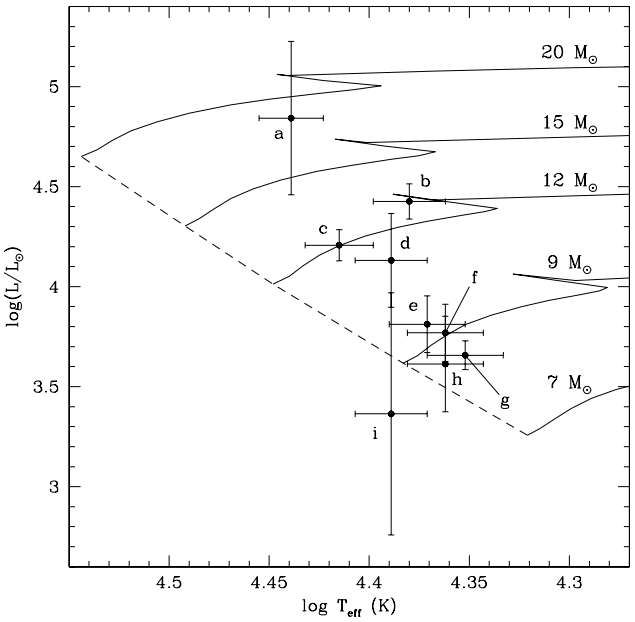

Fig. 5. Position of the programme stars in the HR diagram: (*a*) ξ^1 CMa, (*b*) β CMa, (*c*) β Cep, (*d*) 12 Lac, (*e*) ν Eri, (*f*) δ Cet, (*g*) γ Peg, (*h*) V2052 Oph and (*i*) V836 Cen. The luminosities were computed using *Hipparcos* parallaxes and the bolometric corrections of Flower (1996). The extinction in the V band, A_V, was derived from the theoretical $(B-V)$ colour indices of Bessell et al. (1998). The evolutionary tracks for solar metallicity and without rotation are taken from Schaller et al. (1992). The initial masses are indicated on the right-hand side of this figure. The ZAMS is shown as a dashed line.

that the internal rotation law, $\Omega(r)$, is steeper than currently assumed. A decline of the rotational velocity by a factor 3–5 from the core to the surface has been established from asteroseismological studies in two of our targets: ν Eri (Pamyatnykh et al. 2004) and V836 Cen (Dupret et al. 2004). This appears broadly consistent with the predictions of theoretical models, but this piece of information is unfortunately lacking for the N-rich stars. Additional uncertainties arise from our very limited knowledge of the redistribution of angular momentum in massive pulsating stars (see, e.g. Ando 1983; Lee & Saio 1993). From the observational side, there appears to be an excess of slow rotators among the β Cephei class compared to the global B dwarf population, but an interpretation of this result is made difficult by the fact that stars with low $\Omega R \sin i$ values tend to exhibit photometric changes of larger amplitudes and are hence more easily recognizable as β Cephei variables (Stankov & Handler 2005).

It may be regarded as suggestive that 3 out of the 4 stars with an N excess possess a magnetic field with a longitudinal strength of ∼300 G (ξ^1 CMa; Hubrig et al. 2006) and ∼100 G (V2052 Oph: Neiner et al. 2003; β Cep: Henrichs et al. 2000), whereas similar observations for 3 stars with normal abundances (ν Eri, β CMa and V836 Cen) did not yield any detection (Schnerr et al. 2006; Hubrig et al. 2006). No field has been so far reported in δ Cet (Rudy & Kemp 1978), but much more sensitive observations are being planned (Briquet, private communication). In the models of Maeder & Meynet (2005), magnetic fields tend to enforce near-solid body rotation and therefore to suppress shear mixing. However, meridional circulation is in this case even more efficient at transporting chemical elements from the interior to the surface. Globally, one expects higher N surface abundances, but also the star to rotate faster. The inclusion of magnetic fields does not seem at first glance able to account for the observational data, but the models are still in their infancy and the theoretical predictions sensitive to some ill-defined quantities (e.g. diffusion coefficients). In this regard, we note that the predicted surface enrichments may strongly differ depending on the model considered (Maeder & Meynet 2005; Heger et al. 2005). Furthermore, dynamo action in the radiative layers is assumed to be driven by the so-called Tayler-Spruit instabilities (Spruit 2002), the existence of which is not firmly established and, in any case, poorly constrained from an observational point of view. Perhaps more importantly, complex field geometries are expected in the framework of this model, whereas V2052 Oph and β Cep possess a global dipole field (Neiner et al. 2003; Henrichs et al. 2000). This seems to argue for a magnetic field of fossil origin at least in these two objects. While it might be possible to explain in this context the existence of slowly-rotating magnetic B-type dwarfs depending on their pre-main sequence history (Stępień 2002), a nitrogen enrichment at the surface of such objects remains unexpected. Alternatively, one may postulate that these stars have entered the ZAMS with high rotational velocities, but have experienced a dramatic loss of angular momentum along the main sequence because of magnetic braking. However, this interpretation is very unlikely (see Donati et al. 2001 in the case of β Cep).

One issue which needs to be clarified is whether the observed abundance ratios are only intrinsic to the β Cephei stars or are a characteristic feature of early B-type dwarfs in general. We show in Fig. 7 the NLTE [N/C] and [N/O] ratios for our stars and 34 nearby B1–B2 dwarfs, as a function of $\Omega R \sin i$. When gathering the literature data, we restricted ourselves to stars spanning the same $T_{\rm eff}$ and $\log g$ ranges as our programme stars (see Table 7). In addition, only stars lying at less than about 2 kpc from the Sun were selected to avoid possible [N/C] and [N/O] variations arising from the chemical evolution of the Galaxy (Rolleston et al. 2000). It turns out that as many as 10 stars in this sample are confirmed β Cephei stars (Stankov & Handler 2005). They are plotted, along with our targets, with different symbols in Fig. 7. Great care must be exercised when interpreting these data in view of their heterogeneity, although using line ratios minimizes the systematic errors. The magnitude of this problem can be assessed by comparing the [N/C] and [N/O] ratios for the two stars with independent determinations: HD 61068 (GL; Kilian 1992) and HD 216 916 (GL; Daflon et al. 2001a). The difference is only 0.08 dex on average, but can reach up to 0.19 dex. In spite of the limitations mentioned in Sect. 4.1, we can also compare our results with GL for the seven stars in common. Once again, the differences are small on average (0.12 dex), but are of the order of 0.3 dex in the most extreme case. Table 8 suggests significantly higher mean [N/C] and [N/O] ratios by about 0.25 dex for our subsample of β Cephei stars compared to nearby, presumably non-pulsating B dwarfs (Daflon & Cunha 2004). However, this

is only marginally the case when considering all the data collected from the various sources in the literature shown in Fig. 7 (~0.1 dex). This illustrates the fact that comparing the chemical properties of these two populations at these levels is sensitive to the exact definition of the samples (e.g. evolutionary status) and, most importantly, to systematics in the abundance determinations. Confidently establishing a possible dichotomy between the abundance patterns must await the homogeneous analysis of a large sample. Another more subtle difficulty lies in the fact that stars classified as non pulsating might prove to be β Cephei stars when observed under closer scrutiny (see Telting et al. 2006). We thus conclude at this stage that there is no convincing evidence for a higher amount of mixing in β Cephei stars compared to the global B dwarf population.

We note that only the radial pulsator ξ^1 CMa or the stars dominated by a radial mode, δ Cet, V2052 Oph and β Cep, are N-rich. To further examine the potential role played by pulsations, we have investigated a possible link between the N excesses and several pulsational observables (e.g. velocity amplitudes, oscillation frequencies), but found no correlation between these quantities.

6. Conclusion and prospects

We have presented a detailed, self-consistent determination of the atmospheric parameters and NLTE abundances of nine prototypical β Cephei stars based on very-high quality spectroscopic data covering the entire oscillation cycle in most cases. This study reveals that the abundance patterns are remarkably similar among our sample, with the exception of nitrogen which is enhanced by a factor 2–4 in four targets. Caution should therefore be exercised when considering apparently slowly-rotating, early B-type dwarfs as good tracers of the present-day nitrogen abundance of the interstellar medium, either in the Galaxy or in the Magellanic Clouds. We interpret this nitrogen enrichment, which is systematically accompanied by a boron depletion, as the result of internal mixing. The existence of stars with normal nitrogen abundances, but with a strong boron depletion (e.g. 12 Lac; Fig. 6) supports this conclusion (Fliegner et al. 1996). Mass transfer processes in close binaries can mimic such abundance peculiarities (e.g. Vanbeveren 1989) and/or to lead to a dramatic spin down because of tidal effects (Huang & Gies 2006). However, only two stars in our sample are confirmed members of a (wide) binary system: γ Peg ($\mathcal{P}_{\rm orb}$~370 yr; Chapellier et al. 2006) and β Cep ($\mathcal{P}_{\rm orb}$~90 yr; Pigulski & Boratyn 1992). As γ Peg is not N-enriched, this argues against a binary origin. Furthermore, the other stars have all been the subject of long-term, extensive spectroscopic campaigns (except V836 Cen) and do not present any signs of binarity. For the sake of completeness, we have also computed the peculiar space velocities, $v_{\rm pec}$, of our targets from *Hipparcos* data and found that none of the N-enriched stars exceeds the canonical threshold for a runaway status ($v_{\rm pec} \gtrsim 40$ km s^{-1}; Blaauw 1961). Hence there is no evidence for a dynamical kick imparted by the previous explosion of a putative companion as a supernova. Alternatively, the stars could have formed out of interstellar material contaminated by the ejecta of Type II supernovae. This hypothesis can unfortunately not be tested by comparing the derived abundances with those of OB stars in their immediate vicinity, as none of the four stars is known to be part of an open cluster (Stankov & Handler 2005). Likewise, a search for nearby open clusters with abundance data for early-type members in the WEBDA[6] database proved inconclusive. Nevertheless, such a scenario is unable to explain the boron data and seems very implausible.

At least three N-rich stars (δ Cet, β Cep and V2052 Oph) are intrinsically slow rotators and should not expose such a large amount of core-processed material at their surfaces according to the most recent evolutionary models accounting for rotation. It should be emphasized that the reliability of the theoretical models has so far mainly been tested from observations of OBA supergiants in the Magellanic Clouds (e.g. Trundle & Lennon 2005; Heap et al. 2006 for some recent examples). Studies of B dwarfs, such as the present work, are free of several uncertainties which may render a confrontation between theory and observations difficult for such evolved objects: (a) the uncertainties on the mass-loss rates and on the related loss of angular momentum as the star evolves, (b) their ambiguous evolutionary status (pre- or post-red supergiant phase), and (c) the difficulties in estimating the rotation rate of supergiants (e.g. Dufton et al. 2006). One way of reconciling the model predictions with the observations could be to assume that the $\Omega(r)$ law in the interior is much steeper than hitherto assumed. The existence of a magnetic field in most N-rich stars (Sect. 5.3) indicates that theoretical models including the effect of magnetic fields are probably more relevant for interpreting our observations. A direct comparison with models assuming that the field is produced via dynamo action in the radiative layers (e.g. Maeder & Meynet 2005) may not be appropriate, however, as the fields might be of fossil origin in these objects.

We have determined the abundances of all the chemical species contributing significantly to the global metallicity, Z (except Ne). It is of importance to emphasize that the mild N enrichment observed in some stars has little incidence on the metal content, as this element is only a minor contributor to Z (~5%). As can be seen in Table 8, the metallicity of the studied β Cephei stars is unremarkable and typical of the values observed for early B-type dwarfs in the solar neighbourhood, in accordance with recent works based on UV data (Niemczura & Daszyńska-Daszkiewicz 2005). It can be noticed that the Sun is markedly more metal-rich than young, nearby B stars. This long-standing problem still lacks a clear explanation and may constitute a major source of uncertainty when choosing the appropriate metallicity value in oscillation codes.

Recent multisite, ground-based campaigns have brought a wealth of new high-quality data on β Cephei stars (e.g. Aerts et al. 2004a; Handler et al. 2006), and much more is expected in the near future thanks to a plethora of space missions (e.g. *MOST*, *COROT*, *Kepler*). The diagnostic power of seismic modelling of early-type stars will hence become enormous, but evolution and oscillation codes unfortunately have difficulties in keeping pace with these dramatic observational developments. In particular, concerns have recently been raised

[6] The Database for Galactic Open Clusters (WEBDA) is available online at: `http://www.univie.ac.at/webda/`.

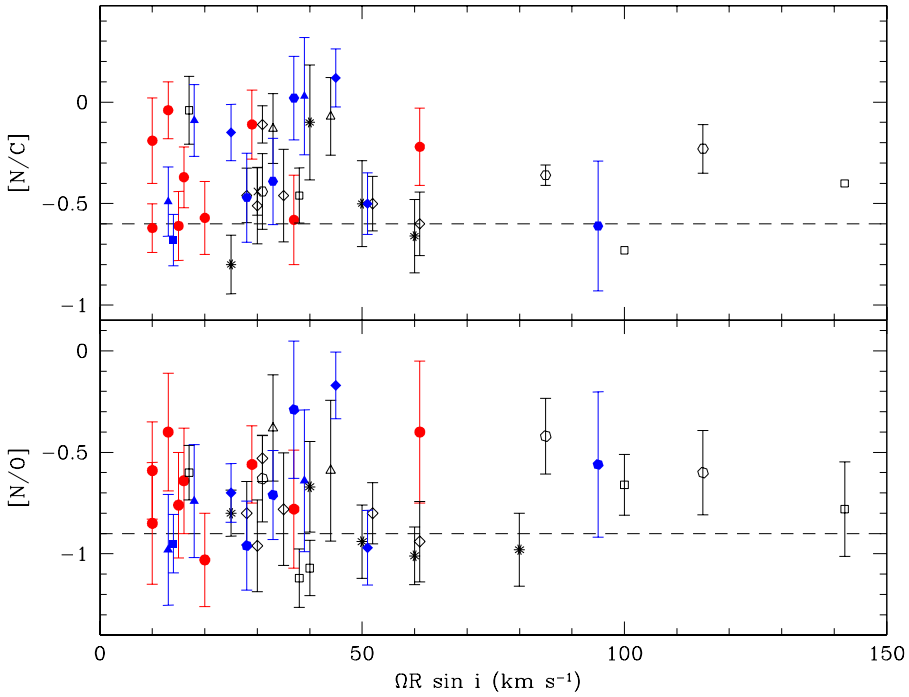

Fig. 7. [N/C] and [N/O] ratios as a function of $\Omega R \sin i$ for our programme stars (*circles*) and a sample of 34 nearby B1–B2 dwarfs: *crosses*: Andrievsky et al. (1999), *squares*: Daflon et al. (1999, 2001a, b), *triangles*: GL, *starred*: Gummersbach et al. (1998), *diamonds*: Kilian (1992) and Kilian et al. (1994), *hexagons*: Mathys et al. (2002). The filled geometrical symbols denote known β Cephei stars (Stankov & Handler 2005). The dashed lines show the typical ratios in the absence of mixing (Table 8). The $\Omega R \sin i$ values from Table 7 have been used for our programme stars. The colour coding in the online version of this journal is the following: *red*: programme stars, *blue*: literature data for other β Cephei stars, *black*: presumably non-pulsating B stars.

regarding the inability of standard models to reproduce the rich oscillation spectrum of 12 Lac and ν Eri. In both cases, the incorporation of gravitational settling and radiative levitation has been claimed as an ad hoc solution to help resolve this problem (Pamyatnykh et al. 2004; Handler et al. 2006). We find that both the [N/C] and the [N/O] ratios are about 0.25 dex above solar in ν Eri (Table 8), a star whose rotation rate only decreases by a factor three between the core and the surface (Pamyatnykh et al. 2004). This is likely significant and provides some indication for deep mixing. Such an interpretation would challenge the existence of diffusion effects at least in this star, as such microscopic processes are known to be severely hindered, or even completely inhibited, by large-scale fluid motions in the interior. However, P.-O. Bourge and collaborators have called our attention to the fact that radiatively-driven microscopic diffusion, and not rotational mixing, could actually be responsible for the N-excess in β Cephei stars. They have already shown that this process can indeed lead to the accumulation of iron in the transition region of β Cephei stars, thus explaining the excitation of all the observed modes in 12 Lac and ν Eri (Bourge & Alecian 2006; Bourge et al. 2006a). Their most recent results show that radiative forces on nitrogen are always greater than those on carbon and oxygen near the surface, thus leading to separation and variable excess of N depending on the stellar parameters (Bourge et al. 2006b). This intriguing possibility opens a new avenue for the interpretation of the abundance peculiarities discussed in this paper.

Acknowledgements. T. M. acknowledges financial support from the European Space Agency through a Postdoctoral Research Fellow grant and from the Research Council of Leuven University through grant GOA/2003/04. M. B. is Postdoctoral Fellow of the Fund for Scientific Research, Flanders. This work benefited from discussions within the Belgian Asteroseismology Group (BAG). We particularly wish to thank P.-O. Bourge, A. Noels, S. Théado and A. Thoul for sharing with us their results regarding diffusion. The useful comments from an anonymous referee are greatly acknowledged. We are indebted to D. J. Lennon and C. Trundle for allowing us to implement their Si II model ion in DETAIL. We are also grateful to the many people involved in the acquisition and reduction of the data presented in this paper, as well as F. Favata for support. The archival ELODIE data have been processed within the PLEINPOT environment. We wish to thank P. Prugniel for his help with PLEINPOT and the ELODIE archives. This research made use of NASA's Astrophysics Data System Bibliographic Services, the SIMBAD database operated at CDS, Strasbourg (France) and the WEBDA database operated at the Institute for Astronomy of the University of Vienna.

References

Aerts, C., Waelkens, C., & De Pauw, M. 1994, A&A, 286, 136
Aerts, C. 1996, A&A, 314, 115
Aerts, C., Thoul, A., Daszyńska, J., et al. 2003, Sci, 300, 1926
Aerts, C., De Cat, P., Handler, G., et al. 2004a, MNRAS, 347, 463
Aerts, C., Waelkens, C., Daszyńska-Daszkiewicz, J., et al. 2004b, A&A, 415, 241
Aerts, C., Marchenko, S. V., Matthews, J. M., et al. 2006, ApJ, 642, 470

Ando, H. 1983, PASJ, 35, 343
Andrievsky, S. M., Korotin, S. A., Luck, R. E., & Kostynchuk, L. Yu. 1999, A&A, 350, 598
Asplund, M., Grevesse, N., & Sauval, A. J. 2005, in Cosmic abundances as records of stellar evolution and nucleosynthesis, ed. T. G. Barnes III & F. N. Bash, ASP Conf. Ser., 336, 25
Aufdenberg, J. P., Hauschildt, P. H., & Baron, E. 1999, MNRAS, 302, 599
Ausseloos, M., Scuflaire, R., Thoul, A., & Aerts, C. 2004, MNRAS, 355, 352
Ausseloos, M. 2005, Ph. D. Thesis, Katholieke Universiteit Leuven, Belgium
Baglin, A. 2003, AdSpR, 31, 345
Baranne, A., Queloz, D., Mayor, M., et al. 1996, A&AS, 119, 373
Becker, S. R., & Butler, K. 1988, A&A, 201, 232
Becker, S. R., & Butler, K. 1989, A&A, 209, 244
Becker, S. R., & Butler, K. 1990, A&A, 235, 326
Becker, S. R. 1998, in Boulder-Munich II: Properties of Hot, Luminous Stars, ed. I. D. Howarth, ASP Conf. Ser., 131, 137
Beeckmans, F., & Burger, M. 1977, A&A, 61, 815
Bessell, M. S., Castelli, F., & Plez, B. 1998, A&A, 333, 231
Blaauw, A. 1961, Bull. Astron. Inst. Netherlands, 15, 265
Bouret, J.-C., Lanz, T., Hillier, D. J., et al. 2003, ApJ, 595, 1182
Bouret, J.-C., Lanz, T., & Hillier, D. J. 2005, A&A, 438, 301
Bourge, P.-O., & Alecian, G. 2006, in Astrophysics of Variable Stars, ed. C. Sterken & C. Aerts, ASP Conf. Ser., 349, 201
Bourge, P.-O., Alecian, G., Thoul, A., Scuflaire, R., & Théado, S. 2006a, CoAst, 147, 105
Bourge, P.-O., Théado, S., & Thoul, A. 2006b, MNRAS, submitted
Butler, K. 1984, Ph. D. Thesis, University of London, UK
Chapellier, E., Le Contel, D., Le Contel, J. M., Mathias, P., & Valtier, J.-C. 2006, A&A, 448, 697
Claret, A. 2000, A&A, 363, 1081
Code, A. D., Davis, J., Bless, R. C., & Brown, R. H. 1976, ApJ, 203, 417
Crowther, P. A. 1998, in Fundamental Stellar Properties: The Interaction between Observation and Theory, ed. T. R. Bedding et al. (Dordrecht: Reidel), IAU Symp., 189, 137
Daflon, S., Cunha, K., & Becker, S. R. 1999, ApJ, 522, 950
Daflon, S., Cunha, K., Becker, S. R., & Smith, V. V. 2001a, ApJ, 552, 309
Daflon, S., Cunha, K., Butler, K., & Smith, V. V. 2001b, ApJ, 563, 325
Daflon, S., Cunha, K., & Butler, K. 2004, ApJ, 604, 362
Daflon, S., & Cunha, K. 2004, ApJ, 617, 1115
Deng, L., & Xiong, D. R. 2001, MNRAS, 327, 881
De Ridder, J., Dupret, M.-A., Neuforge, C., & Aerts, C. 2002, A&A, 385, 572
Desmet, M., Briquet, M., Mazumdar, A., & Aerts, C. 2006, CoAst, 147, 113
Donati, J.-F., Wade, G. A., Babel, J., et al. 2001, MNRAS, 326, 1265
Drew, J. E., Denby, M., & Hoare, M. G. 1994, MNRAS, 266, 917
Dufton, P. L., Brown, P. J. F., Lennon, D. J., & Lynas-Gray, A. E. 1986, MNRAS, 222, 713
Dufton, P. L., Ryans, R. S. I., Trundle, C., et al. 2005, A&A, 434, 1125
Dufton, P. L., Ryans, R. S. I., Simón-Díaz, S., Trundle, C., Lennon, D. J. 2006, A&A, 451, 603
Dupret, M.-A., Thoul, A., Scuflaire, R., et al. 2004, A&A, 415, 251
Eber, F., & Butler, K. 1988, A&A, 202, 153
Fitzpatrick, E. L., & Massa, D. 2005, AJ, 129, 1642
Fliegner, J., Langer, N., & Venn, K. A. 1996, A&A, 308, L13
Flower, P. J. 1996, ApJ, 469, 355
Giddings, J. R. 1981, Ph. D. Thesis, University of London, UK
Gies, D. R., & Lambert, D. L. 1992, ApJ, 387, 673 (GL)
Gold, M. 1984, Diplomarbeit, Ludwig Maximilian Universität, München, Germany
Gray, D. F. 1976, The Observation and Analysis of Stellar Photospheres (Wiley-Interscience)
Grevesse, N, & Sauval, A. J. 1998, Space Sci. Rev., 85, 161
Gummersbach, C. A., Kaufer, A., Schäfer, D. R., Szeifert, T., & Wolf, B. 1998, A&A, 338, 881
Hambly, N. C., Dufton, P. L., Keenan, F. P., & Lumsden, S. L. 1996, MNRAS, 278, 811
Handler, G., Jerzykiewicz, M., Rodríguez, E., et al. 2006, MNRAS, 365, 327
Heap, S. R., Lanz, T., & Hubeny, I. 2006, ApJ, 638, 409
Heger, A., & Langer, N. 2000, ApJ, 544, 1016
Heger, A., Woosley, S. E., & Spruit, H. C. 2005, ApJ, 626, 350
Henrichs, H. F., de Jong, J. A., Donati, J.-F., et al. 2000, in The Be Phenomenon in Early-Type Stars, ed. M. A. Smith, H. F. Henrichs, & J. Fabregat, ASP Conf. Ser., 214, 324
Herrero, A., & Lennon, D. J. 2004, in Stellar Rotation, ed. A. Maeder & P. Eenens, ASP Conf. Ser., 215, 209
Heynderickx, D., Waelkens, C., & Smeyers, P. 1994, A&AS, 105, 447
Hillier, D. J., & Miller, D. L. 1998, ApJ, 496, 407
Huang, W., & Gies, D. R. 2006, ApJ, in press (astro-ph/0510720)
Hubeny, I., & Lanz, T. 1995, ApJ, 439, 875
Hubrig, S., Briquet, M., Schöller, M., et al. 2006, MNRAS, 369, L61
Husfeld, D., Butler, K., Heber, U., & Drilling, J. S. 1989, A&A, 222, 150
Jerzykiewicz, M., Handler, G., Shobbrook, R. R., et al. 2005, MNRAS, 360, 619
Kilian, J. 1992, A&A, 262, 171
Kilian, J., Montenbruck, O., & Nissen, P. E. 1994, A&A, 284, 437
Kołaczkowski, Z., Pigulski, A., Soszyński, I., et al. 2004, in Variable Stars in the Local Group, ed. D. W. Kurtz & K. Pollard, ASP Conf. Ser., 310, 225
Korotin, S. A., Andrievsky, S. M., & Kostynchuk, L. Yu. 1999a, Ap&SS, 260, 531
Korotin, S. A., Andrievsky, S. M., & Kostynchuk, L. Yu. 1999b, A&A, 342, 756
Korotin, S. A., Andrievsky, S. M., & Luck, R. E. 1999c, A&A, 351, 168
Kupka, F., Piskunov, N., Ryabchikova, T. A., Stempels, H. C., & Weiss, W. W. 1999, A&AS, 138, 119
Kurucz, R. L. 1979, ApJS, 40, 1
Kurucz, R. L. 1993, ATLAS9 Stellar Atmosphere Programs and 2 km/s grid. Kurucz CD-ROM No. 13. Cambridge, Mass.: Smithsonian Astrophysical Observatory, 1993, 13
Lamers, H. J. G. L. M., & Achmad, L. 1994, A&A, 291, 856
Lee, U., & Saio, H. 1993, MNRAS, 261, 415
Lennon, D. J., Dufton, P. L., & Crowley, C. 2003, A&A, 398, 455
Lyubimkov, L. S., Rachkovskaya, T. M., Rostopchin, S. I., & Lambert, D. L. 2002, MNRAS, 333, 9
Lyubimkov, L. S., Rostopchin, S. I., & Lambert, D. L. 2004, MNRAS, 351, 745
Maeder, A., & Meynet, G. 2005, A&A, 440, 1041
Martin, J. C. 2004, AJ, 128, 2474
Martins, F., Schaerer, D., Hillier, D. J., et al. 2005, A&A, 441, 735
Mathys, G., Andrievsky, S. M., Barbuy, B., Cunha, K., & Korotin, S. A. 2002, A&A, 387, 890
Mazumdar, A., Briquet, M., Desmet, M., & Aerts, C. 2006, A&A, in press
Mendel, J. T., Venn, K. A., Proffitt, C. R., Brooks, A. M., & Lambert, D. L. 2006, ApJ, 640, 1039
Meynet, G., & Maeder, A. 2000, A&A, 361, 101
Meynet, G., & Maeder, A. 2003, A&A, 404, 975

Mokiem, M. R., de Koter, A., Puls, J., et al. 2005, A&A, 441, 711
Morton, A. E., & Hansen, H. K. 1974, PASP, 86, 943
Moultaka, J., Ilovaisky, S. A., Prugniel, P., & Soubiran, C. 2004, PASP, 116, 693
Neiner, C., Henrichs, H. F., Floquet, M., et al. 2003, A&A, 411, 565
Niemczura, E., & Daszyńska-Daszkiewicz, J. 2005, A&A, 433, 659
Nieva, M. F., & Przybilla, N. 2006, ApJ, 639, L39
Olive, K. A., & Skillman, E. D. 2004, ApJ, 617, 29
Pamyatnykh, A. A. 1999, Acta Astron., 49, 119
Pamyatnykh, A. A., Handler, G., & Dziembowski, W. A. 2004, MNRAS, 350, 1022
Peters, G. J. 1973, PASP, 85, 536
Pigulski, A., & Boratyn, D. A. 1992, A&A, 253, 178
Proffitt, C. R., & Quigley, M. F. 2001, ApJ, 548, 429
Przybilla, N., Butler, K., Becker, S. R., & Kudritzki, R. P. 2001, A&A, 369, 1009
Przybilla, N., Butler, K., Becker, S. R., & Kudritzki, R. P. 2006, A&A, 445, 1099
Puls, J., Urbaneja, M. A., Venero, R., et al. 2005, A&A, 435, 669
Rolleston, W. R. J., Smartt, S. J., Dufton, P. L., & Ryans, R. S. I. 2000, A&A, 363, 537
Rolleston, W. R. J., Venn, K., Tolstoy, E., Dufton, P. L. 2003, A&A, 400, 21
Rudy, R. J., & Kemp, J. C. 1978, MNRAS, 183, 595
Saesen, S., Briquet, M., & Aerts, C. 2006, CoAst, 147, 109
Schaller, G., Schaerer, D., Meynet, G., & Maeder, A. 1992, A&AS, 96, 269
Schnerr, R. S., Verdugo, E., Henrichs, H. F., & Neiner, C. 2006, A&A, 452, 969
Smalley, B., & Dworetsky, M. M. 1995, A&A, 293, 446
Spruit, H. C. 2002, A&A, 381, 923
Stankov, A., & Handler, G. 2005, ApJS, 158, 193
Stępień, K. 2002, A&A, 383, 218
Telting, J. H., Aerts, C., & Mathias, P. 1997, A&A, 322, 493
Telting, J. H., Schrijvers, C., Ilyin, I. V., et al. 2006, A&A, 452, 945
Trundle, C., Lennon, D. J., Puls, J., & Dufton, P. L. 2004, A&A, 417, 217
Trundle, C., & Lennon, D. J. 2005, A&A, 434, 677
Urbaneja, M. A., Herrero, A., Bresolin, F., et al. 2003, ApJ, 584, L73
Vanbeveren, D. 1989, A&A, 224, 93
vander Linden, D., & Butler, K. 1988, A&A, 189, 137
Venn, K. A., Brooks, A. M., Lambert, D. L., et al. 2002, ApJ, 565, 571
Vrancken, M., Butler, K., & Becker, S. R. 1996, A&A, 311, 661
Vrancken, M. 1997, Ph. D. Thesis, Vrije Universiteit Brussel, Belgium
Watson, R. D. 1971, ApJ, 169, 343
Watson, R. D. 1972, ApJS, 24, 167
Zhai, M., & Shaw, D. M. 1994, Meteoritics, 29, 607

Online Material

Appendix A: EW measurements

Table A.1 lists the measured EWs for the studied stars. Our EWs are systematically larger than the values quoted by GL for the seven stars in common, but a similar trend is evident when comparing their values with previous measurements in the literature (see their Fig. 4). This is likely to result from their use of Gaussian fitting instead of the direct integration used in our case. The same conclusion holds for the EWs of ξ^1 CMa presented by Hambly et al. (1996).

List of Objects

‘γ Peg’ on page 1
‘δ Cet’ on page 1
‘ν Eri’ on page 1
‘β CMa’ on page 1
‘ξ^1 CMa’ on page 1
‘V836 Cen’ on page 1
‘V2052 Oph’ on page 1
‘β Cep’ on page 1
‘12 Lac’ on page 1
‘β Cep’ on page 1
‘V2052 Oph’ on page 1
‘δ Cet’ on page 1
‘ξ^1 CMa’ on page 1
‘12 Lac’ on page 2
‘ν Eri’ on page 2
‘ν Eri’ on page 2
‘V836 Cen’ on page 2
‘γ Peg’ on page 2
‘δ Cet’ on page 2
‘ν Eri’ on page 2
‘β CMa’ on page 2
‘ξ^1 CMa’ on page 2
‘V836 Cen’ on page 2
‘V2052 Oph’ on page 2
‘β Cep’ on page 2
‘12 Lac’ on page 2
‘ν Eri’ on page 2
‘ν Eri’ on page 2
‘β CMa’ on page 2
‘ξ^1 CMa’ on page 2
‘V836 Cen’ on page 2
‘V2052 Oph’ on page 2
‘12 Lac’ on page 2
‘δ Cet’ on page 2
‘γ Peg’ on page 2
‘β Cep’ on page 2
‘V836 Cen’ on page 2
‘γ Peg’ on page 3
‘δ Cet’ on page 3
‘ν Eri’ on page 3
‘β CMa’ on page 3
‘ξ^1 CMa’ on page 3
‘V836 Cen’ on page 3
‘V2052 Oph’ on page 3
‘β Cep’ on page 3
‘12 Lac’ on page 3
‘HD 886’ on page 3
‘HD 16582’ on page 3
‘HD 29248’ on page 3
‘HD 44743’ on page 3
‘HD 46328’ on page 3
‘HD 129 929’ on page 3
‘HD 163 472’ on page 3
‘HD 205 021’ on page 3
‘HD 214 993’ on page 3
‘β CMa’ on page 3
‘ξ^1 CMa’ on page 3
‘V2052 Oph’ on page 3
‘β CMa’ on page 3
‘HD 35299’ on page 4
‘β Cep’ on page 4
‘ξ^1 CMa’ on page 4
‘β CMa’ on page 4
‘γ Peg’ on page 4
‘ξ^1 CMa’ on page 4
‘β CMa’ on page 4
‘β CMa’ on page 4
‘β Cep’ on page 4
‘β Cep’ on page 5
‘β CMa’ on page 5
‘V2052 Oph’ on page 5
‘12 Lac’ on page 5
‘β CMa’ on page 5
‘ξ^1 CMa’ on page 5
‘β Cep’ on page 5
‘12 Lac’ on page 5
‘β CMa’ on page 5
‘ξ^1 CMa’ on page 5
‘β Cep’ on page 5
‘ξ^1 CMa’ on page 5
‘β Cep’ on page 5
‘β CMa’ on page 6
‘β CMa’ on page 6
‘V2052 Oph’ on page 6
‘β Cep’ on page 6
‘V2052 Oph’ on page 6
‘V836 Cen’ on page 6
‘V836 Cen’ on page 7
‘V2052 Oph’ on page 7
‘γ Peg’ on page 7
‘δ Cet’ on page 7
‘ν Eri’ on page 7
‘β CMa’ on page 7
‘ξ^1 CMa’ on page 7
‘V836 Cen’ on page 7
‘V2052 Oph’ on page 7
‘β Cep’ on page 7
‘12 Lac’ on page 7
‘β Cep’ on page 7
‘V2052 Oph’ on page 7
‘β CMa’ on page 7
‘ξ^1 CMa’ on page 7
‘β Cep’ on page 7

Table A.1. EW measurements in mÅ. A blank may have various causes: the EW was not reliably measurable (spectral features lying in the wings of the Balmer and diffuse He I lines were avoided); the line fell into echelle inter-order gaps; was considered blended for the relevant temperature range; or yielded a discrepant abundance. The latter point notably applies to the C II λ4267 line which is notoriously known to yield spuriously low abundances (e.g. Lennon et al. 2003, although Nieva & Przybilla 2006 appear to have recently solved this problem).

Transition[a]	γ Peg	δ Cet	ν Eri	β CMa	ξ^1 CMa		V836 Cen	V2052 Oph	β Cep	12 Lac
					Max EWs	Min EWs				
He I										
4026.20	1245	1366	1236	1049	1010	1035	1207	1546	1018	1109
4387.93	838.7	846.5	778.9	648.9	676.8	678.9	741.6	1046	691.7	712.4
4437.55	125.5	134.6		118.7	104.9	104.7	122.7	154.1	86.1	108.1
4471.48	1238	1360			1049	1094	1256		1124	
4713.15	261.4	274.3	290.7	293.1	261.0	258.9	276.0	291.3	242.7	
4921.93	826.9	850.2	820.0	725.1	689.0	705.0	804.3	1131	724.7	764.5
5015.68	289.3	290.5	336.6	352.6	298.7	297.4	296.9	388.9	274.6	330.8
5047.74	168.3	188.9	193.3	182.8	170.5	164.0	181.7	201.3	144.8	169.2
5875.62		775.6	834.1	854.4	749.6	760.0	751.3	839.0		777.3
6678.15	615.7	663.5	735.3	777.9	671.3	679.1	664.5	800.1		709.3
C II										
5133.11	64.2	52.4	69.0	57.0	42.0	36.5	70.1		33.8	
5137.26			10.2	6.5	5.1	4.1			4.6	
5139.17	12.3	10.4	12.2	9.5	7.6	5.3	18.2		6.0	13.0
5143.50				27.1	20.9	17.9	35.8		17.8	25.7
5145.16	54.5	49.2	65.4	68.0	40.0	37.1	59.2		34.8	67.1
5151.08	34.5	29.0	43.7					37.1		
6780.26	44.7	31.4	44.0				54.8	44.4	18.9	39.8
6783.91	47.7	40.1	51.0		31.0	26.9	60.7	46.0	26.0	46.0
6787.21				11.5	7.2	6.8	19.8		8.3	
6791.47	18.5		19.5	13.7	9.5	8.2	25.2	18.2	6.3	
6798.10			3.7							
6800.69	16.2		15.9	11.0	8.0	5.6			7.3	
C III										
4186.90				15.3					16.4	18.4
N II										
3955.85					45.7	40.6				
3995.00					124.2	115.6				
4179.67	8.9	19.7			21.5	23.2	12.6	18.8		
4227.74	15.8	36.8	36.4	22.6	33.7	28.9	25.8	29.0	32.6	21.9
4236.99				43.7	65.0	60.9				
4564.76		3.4								
4607.16	34.4	66.4	61.0	42.7	59.8	50.1	51.6	57.2	57.0	50.9
4643.09	40.3	74.1	82.2	41.6	65.5	55.4	57.7		63.5	43.7
4654.53	6.8	17.1	11.3					12.7		
4667.21	4.2	11.7		4.9					9.6	
4674.91	4.5	12.4							6.9	
4774.24	2.7									
4779.72				11.4	19.9	16.3	15.4		19.8	
4781.19	2.1	6.6	5.0						4.1	
4788.14	14.8	32.7	29.3	20.0	28.2	24.1	21.2		28.8	
4987.38	8.6	17.9	19.4	13.0	14.5	12.6	9.4	18.0	14.5	14.0
4994.36	19.8		44.2	31.6	36.0	31.5	35.1	35.1	34.8	
5001.30				131.0	143.1	127.1	127.7			128.5
5002.70	15.0	32.5	36.2	20.6	30.1	24.3	21.7			17.2
5005.15	51.3	81.1		91.6	90.6	81.8	74.8	70.9		74.6
5007.33				40.1	46.0	40.2	36.0		45.7	36.2

‘ξ^1 CMa’ on page 7
‘V2052 Oph’ on page 7
‘δ Cet’ on page 7
‘ξ^1 CMa’ on page 7
‘γ Peg’ on page 7
‘δ Cet’ on page 7
‘V2052 Oph’ on page 7
‘β CMa’ on page 7
‘γ Peg’ on page 8
‘δ Cet’ on page 8
‘ν Eri’ on page 8
‘β CMa’ on page 8
‘ξ^1 CMa’ on page 8
‘V836 Cen’ on page 8
‘V2052 Oph’ on page 8
‘β Cep’ on page 8
‘12 Lac’ on page 8
‘β CMa’ on page 8
‘γ Peg’ on page 9
‘β CMa’ on page 9
‘V836 Cen’ on page 9
‘12 Lac’ on page 9
‘δ Cet’ on page 9
‘ξ^1 CMa’ on page 9
‘V2052 Oph’ on page 9
‘β Cep’ on page 9
‘ν Eri’ on page 9
‘ξ^1 CMa’ on page 9
‘β Cep’ on page 9
‘δ Cet’ on page 10
‘β Cep’ on page 10
‘12 Lac’ on page 10

Transition[a]	γ Peg	δ Cet	ν Eri	β CMa	ξ^1 CMa		V836 Cen	V2052 Oph	β Cep	12 Lac
					Max EWs	Min EWs				
N II (Continued)										
5010.62	26.7	53.8	66.5	54.0	54.2	43.7	41.9			
5011.31					7.0	4.7				
5012.04		8.8			12.5	10.8				
5025.66		22.0		19.6	17.4	15.1	14.9			22.5
5045.10				65.1	74.8	62.6	63.0			65.0
5462.58					8.8	8.0				
5480.05	3.9	10.3	10.8		11.9	9.5				
5495.65	12.9	24.0	28.3	24.8	30.2	25.6	23.1		30.9	26.0
5551.92					4.8	4.8				
5666.63		84.9		74.1	83.6	69.4	72.9	66.4	83.7	70.1
5676.02	32.0	63.2	71.7	58.8	72.1	61.3	58.3	53.4	69.4	54.6
5679.56	69.1	113.7		130.1	125.6	109.2	108.2	100.4		112.9
5686.21	24.9	52.1	55.4	38.0	45.6	36.0	42.7		53.0	44.6
5710.77	25.1	51.3	50.1	40.5	49.7	41.6	39.9		48.1	37.3
5747.30	8.0	22.3	15.8	8.8	17.2	14.3				
5767.45		12.0	7.3		7.9	6.8				
6242.41				5.8	12.3	9.9			12.7	
6379.62	10.0	22.3	19.9	11.7	16.7	11.9			18.7	22.9
N III										
4634.13				9.3	26.9	34.9			18.1	
O II										
3912.04	45.2	54.5	79.8	129.7	117.0	109.1	83.0	50.7	100.0	99.1
4069.75	92.8	110.4	181.3	272.9			167.9	92.5	200.5	178.5
4072.15				203.9	144.3	139.8	103.9			
4078.86				87.4	68.5	65.0			52.9	
4084.88					107.4	103.2				
4129.31				31.1	25.6	24.4				
4132.79				102.9	84.5	84.6	56.6		68.7	
4185.44	29.5	33.1	54.5		79.7	79.2	54.4	31.2	64.3	63.4
4283.33							65.4			
4319.78				182.8	142.1	134.6			113.4	
4366.70	58.4	61.6	118.7	175.8	136.8	130.0	91.9	56.8	118.5	
4414.88	73.9	81.5	151.7	231.5	179.6	173.2	120.0	67.6	161.4	150.0
4416.97				185.9	152.1	147.4	106.5		138.4	120.3
4452.38	28.5	31.2	54.1	84.0	72.9	70.1	53.2		63.6	59.8
4591.01	47.7	53.5	99.0	166.3	135.4	131.0	86.9	48.5	116.2	103.0
4596.07	48.3	51.5	91.1	152.5	133.5	127.9	86.9	48.9	112.9	104.4
4609.79					108.6	110.7	77.7		91.7	76.1
4641.82	72.6	85.0	163.8	249.0	186.6	180.7	121.8		162.9	193.1
4649.14	90.7	101.3			219.1	211.2	156.0	73.4		223.3
4661.64	53.5	59.3	113.0	182.1	141.5	135.1	95.7	53.2	121.0	117.5
4673.75				68.6	56.6	55.5	33.0		46.0	42.7
4676.24	45.4	49.0		166.3	119.6	114.7	78.2	52.0	106.6	114.3
4691.15	8.7		15.1	25.1	26.7	25.4		10.3	20.9	19.9
4696.36	13.0	16.1	23.5	38.6	35.8	32.2			30.2	23.0
4701.44	13.4	14.9	24.6	41.0	43.4	41.9	28.7		33.7	28.2
4705.32	42.5	46.2	80.2	136.3	114.4	111.6	80.5	33.3	97.2	
4741.70	5.1	4.7		15.0	16.3	15.1			12.4	
4890.85				43.6	39.0	36.4			33.1	
4906.82	20.4	23.2	43.1	73.4	63.1	60.4	41.9	21.4	56.7	42.7
4941.10	17.6	23.8	39.7	64.0	55.9	55.6	38.3	20.9	47.1	55.9
4943.00					80.0	79.9	55.1		70.1	71.1
4955.74	8.2	10.6	19.2	32.6	27.7	26.8			23.4	19.6
5175.99				18.9						

‘δ Cet’ on page 10
‘ν Eri’ on page 10
‘V836 Cen’ on page 10
‘δ Cet’ on page 10
‘β CMa’ on page 10
‘12 Lac’ on page 10
‘V2052 Oph’ on page 10
‘β Cep’ on page 10
‘ξ^1 CMa’ on page 10
‘δ Cet’ on page 10
‘V2052 Oph’ on page 10
‘β Cep’ on page 10
‘ν Eri’ on page 10
‘V836 Cen’ on page 10
‘ξ^1 CMa’ on page 11
‘β CMa’ on page 11
‘β Cep’ on page 11
‘12 Lac’ on page 11
‘ν Eri’ on page 11
‘δ Cet’ on page 11
‘γ Peg’ on page 11
‘V2052 Oph’ on page 11
‘V836 Cen’ on page 11
‘ξ^1 CMa’ on page 11
‘V2052 Oph’ on page 11
‘β Cep’ on page 11
‘ν Eri’ on page 11
‘β CMa’ on page 11
‘V836 Cen’ on page 11
‘δ Cet’ on page 11
‘V2052 Oph’ on page 11
‘β Cep’ on page 11
‘β Cep’ on page 11
‘HD 61068’ on page 11
‘HD 216 916’ on page 11
‘ξ^1 CMa’ on page 12

Transition[a]	γ Peg	δ Cet	ν Eri	β CMa	ξ^1 CMa		V836 Cen	V2052 Oph	β Cep	12 Lac
					Max EWs	Min EWs				
O II (Continued)										
5190.56	7.2				28.5	26.7				
5206.71				57.8	51.8	49.7	30.9		42.8	
6640.99			33.7	62.1	61.3	57.2			47.7	36.8
6721.36			49.2	95.9	84.7	78.0	47.1		71.0	
Mg II										
4481.20	156.1	160.5	205.8	170.3	133.7	127.8	161.8	149.0[b]	134.4	166.0
4739.65				3.8						
7877.05							44.5			
7896.20							53.8			
Al III										
4149.94	34.4	33.5	46.2	28.1	26.9	23.9	37.0	27.1	19.8	
4479.93	40.3	46.6	51.7	53.5	40.7	36.7	61.4		41.8	54.9
4512.56	38.2	40.6	52.7	47.7	37.2	33.0	48.2	38.1	31.7	46.0
4529.07	62.9	66.9	90.8	85.0	60.3	54.7	76.6		53.8	87.6
Si II										
4128.05		34.0	61.5	33.4			33.1	41.1		
4130.89	35.8	40.8	59.8	25.0			31.1		10.8	
5056.15			25.3							
6371.37	40.1	29.8	23.4				23.2			
Si III										
4567.84	100.7	112.9	215.5	277.1			145.5	100.5	173.8	202.1
4574.76	67.8	77.1	139.2	180.9			101.9	66.5	117.7	134.7
4813.33	21.6		42.5	53.8	43.4	37.4	35.5	23.1	38.1	41.1
4819.77				82.7			62.6		59.8	67.3
4829.07			55.9	77.1	63.7	58.2	53.9	38.3	55.4	
5716.29									4.6	
5739.73	72.7	82.0	174.5	223.7			119.5	84.7	137.3	166.6
Si IV										
4212.40				9.5	18.8	23.0			10.4	4.6
6701.21					8.6	12.4				
S II										
4162.48	29.0	26.0	30.4					39.5		
4174.13	22.5	23.1						30.6		
4217.18	4.8		5.4					5.7		
4230.94	4.9							5.9		
4269.72	4.8									
4456.38	2.7									
4483.43	6.7									
4486.63	2.8									
4524.81	11.9	14.7	11.8				12.3			
4656.76	5.3									
4668.50	4.1									
4755.02	4.2									
4763.31	2.3									
4792.01	5.3		4.7							
4815.55		24.6	22.6	15.3			18.4	26.6	5.7	11.7
S III										
4361.53				57.0	49.4	44.7			37.3	35.3
4527.91					4.9	5.3				
Fe III										
4005.04	17.1									16.9
4081.01		17.4			20.9	19.2				
4122.78		17.2			19.1	16.0				
4137.76	19.0	20.9					31.2			

‘δ Cet’ on page 12
‘V2052 Oph’ on page 12
‘β Cep’ on page 12
‘12 Lac’ on page 12
‘γ Peg’ on page 12
‘β Cep’ on page 12
‘γ Peg’ on page 12
‘V836 Cen’ on page 12
‘δ Cet’ on page 12
‘β Cep’ on page 12
‘V2052 Oph’ on page 12
‘12 Lac’ on page 12
‘ν Eri’ on page 12
‘ν Eri’ on page 12
‘12 Lac’ on page 13
‘ν Eri’ on page 13
‘ξ^1 CMa’ on page 2
‘γ Peg’ on page 3
‘δ Cet’ on page 3
‘ν Eri’ on page 3
‘β CMa’ on page 3
‘ξ^1 CMa’ on page 3
‘V836 Cen’ on page 3
‘V2052 Oph’ on page 3
‘β Cep’ on page 3
‘12 Lac’ on page 3
‘γ Peg’ on page 4
‘δ Cet’ on page 4
‘ν Eri’ on page 4
‘β CMa’ on page 4
‘ξ^1 CMa’ on page 4
‘V836 Cen’ on page 4
‘V2052 Oph’ on page 4
‘β Cep’ on page 4
‘12 Lac’ on page 4
‘γ Peg’ on page 5

Transition[a]	γ Peg	δ Cet	ν Eri	β CMa	ξ^1 CMa		V836 Cen	V2052 Oph	β Cep	12 Lac
					Max EWs	Min EWs				
Fe III (Continued)										
4139.35	17.6						31.4			
4154.96	5.3	6.0								
4164.82				66.2	56.1	51.1	58.4		51.7	69.0
4166.84	13.6				16.1	14.3	20.7		18.5	22.2
4222.27		21.5	31.1							
4248.77	4.8		7.7							
4261.39	5.3	5.1			4.5	4.3		3.6	4.2	5.7
4296.85	11.3			23.6	19.9	16.8		12.1	20.0	21.9
4310.35	15.2		36.7	34.7	27.8	23.3	27.6	14.0	21.4	27.4
4419.60	32.7	34.2	52.4	44.0	30.6	22.5	44.8	27.8		38.9
4431.02	23.7	24.3								
5063.42	10.1	9.2	12.7	9.0	6.3	3.2	10.6	12.6		
5086.70			25.2	17.3	12.7	9.1	20.9	25.2	19.3	27.8
5127.51				54.3	44.8	33.1	61.8		38.3	
5136.11				3.3	3.6	2.3				
5156.11	38.4	37.5	59.9	51.8	38.2	30.4		37.6	36.4	53.2
5193.91		19.0		24.0				16.5	16.1	29.1
5218.10					8.2	5.5				
5235.66	11.6	12.7	33.4	25.9	18.1	11.3	22.2		19.3	32.6
5243.31				51.7	41.9	34.1				57.6
5276.48				32.3	25.0	19.0	26.8		22.1	36.9
5282.30	16.5	20.5	40.3	38.2	27.2	19.5	34.0		28.5	39.1
5284.83	5.6		12.5	13.8	9.8	7.8				
5298.11	4.7	6.3	12.1	12.2	8.0	5.3			8.9	12.4
5299.93	11.5	13.3	24.0	21.8	15.6	11.0	22.3		15.1	28.6
5302.60	13.2	15.6		25.6	19.4	15.1	20.8		19.1	25.9
5306.76				18.6	13.3	9.0	14.3		14.4	20.1
5310.88					6.7	4.4			7.8	
5322.74	3.3				5.8	5.0			7.6	9.1
5363.56				12.3	9.9	7.7			8.1	
5460.80	7.6	8.5		8.6	7.8	5.6				
5485.52	7.6	7.8	12.3	10.9					8.1	
5573.42	8.4		13.7	12.7	10.1	7.1	14.3	10.5	11.5	17.7
5744.21					7.4	5.2				
5756.39			11.4							
5833.94			79.2	80.1						78.2
5848.76				11.9					12.1	
5854.62	6.5	9.2			11.6	9.3				
6032.64	13.0	13.8								
6036.55	6.5	8.1			10.6	8.2				
6048.53	6.6		25.2						18.3	22.5
6054.36	5.3				7.7	5.3				

[a] The mean wavelength is given.
[b] Corrected for the contribution of Al III λ4479.93 estimated from spectral synthesis.

‘δ Cet’ on page 5
‘ν Eri’ on page 5
‘β CMa’ on page 5
‘ξ^1 CMa’ on page 5
‘V836 Cen’ on page 5
‘V2052 Oph’ on page 5
‘β Cep’ on page 5
‘12 Lac’ on page 5
‘γ Peg’ on page 6
‘δ Cet’ on page 6
‘ν Eri’ on page 6
‘β CMa’ on page 6
‘ξ^1 CMa’ on page 6
‘V836 Cen’ on page 6
‘V2052 Oph’ on page 6
‘β Cep’ on page 6
‘12 Lac’ on page 6